Role of Chloroplast Lipid-Remodelling Protein 23 During Cold Acclimation in *Arabidopsis thaliana*

Wing Tung Lo (盧泳彤)[1], Denise Winkler[1], Maximilian Münch[1], Martin Lehmann[1,2], Kira Steiner[1], Bettina Bölter[3], Cecilia Tullberg[4], Carl Grey[4], Tatjana Kleine[1], Eslam Abdel-Salam[1], Katharina W. Ebel[5], H. Ekkehard Neuhaus[5], Deren Büyüktaş[6], Sophie de Vries[6], Hans-Henning Kunz[3], Dario Leister [1,2], Serena Schwenkert [1,2]*

[1]Plant Molecular Biology, LMU München, Großhaderner Str. 2-4, 82152, Planegg, Germany.

[2]Mass Spectrometry of Biomolecules (MSBioLMU), LMU München, Großhaderner Straße 2-4, 82152 Martinsried-Planegg, Germany.

[3]Plant Biochemistry and Physiology, LMU München, Großhaderner Straße 2-4, 82152 Martinsried-Planegg, Germany.

[4]Division of Biotechnology, Department of Chemistry, Lund University, Naturvetarvägen 16, 22100 Lund, Sweden

[5]Plant Physiology, University of Kaiserslautern, Paul-Ehrlich-Str., 67663 Kaiserslautern, Germany.

[6]Department of Applied Bioinformatics, Institute of Microbiology and Genetics, University of Goettingen, Goldschmidtstraße 1, 37077 Goettingen, Germany

*Corresponding author: Serena Schwenkert, serena.schwenkert@lmu.de

Short title: Role of CLRP23 in cold acclimation

The author responsible for distribution of materials integral to the findings presented in this article in accordance with the policy described in the Instructions for Authors (https://academic.oup.com/plcell/pages/General-Instructions) is: Serena Schwenkert (serena.schwenkert@lmu.de).

Abstract

Cold acclimation is a crucial physiological process that enables plants to adapt to low temperatures. A key aspect of this adaptation is lipid remodelling, which preserves membrane fluidity and integrity under cold stress. Proteins of the chloroplast envelope membranes are increasingly recognized for their role in acclimation to changing environmental conditions. While lipid synthesis occurs at the inner envelope membrane—where monogalactosyldiacylglycerol synthase is one of the few inner envelope proteins known to face the intermembrane space—little is known about specific proteins involved in lipid remodelling during cold acclimation. In this study, we investigate the role of Chloroplast Lipid Remodelling Protein 23 (CLRP23) as a component of the inner chloroplast envelope membrane. Subcellular fractionation combined with protease protection assays provided evidence for its orientation toward the intermembrane space. To explore its function, we analysed the physiological performance and lipid composition in CLRP23-deficient mutant plants. Under cold stress, we observed significant impairments in photosynthesis and exaggerations in galactolipid response, suggesting CLRP23 is involved in lipid remodelling. Docking analysis suggests CLRP23 may bind to galactolipids, thereby modulating their composition and saturation status. Complemented by transcriptomic and proteomic analyses, these findings expand our understanding of protein-mediated processes during cold acclimation.

Introduction

Chloroplasts, like all plastids, trace their origins to an ancient endosymbiotic event involving the engulfment of a free-living cyanobacteria-like prokaryote by an ancient host cell. As a result of this evolutionary history, chloroplasts are bound by a double-membrane consisting of the outer (OE) and inner (IE) envelope, which are separated by an intermembrane space (IMS; Dyall et al., 2004). In higher plants, chloroplasts not only serve as the cellular site of photosynthesis but also house the enzymatic machinery necessary for various interconnected pathways that are central to plant metabolism (Weber and Fischer, 2009).

As the interface that separates the chloroplast from the cytosol, the chloroplast envelope is a highly complex and dynamic membrane system (Block et al., 2007). The evolution of chloroplasts from ancient cyanobacteria involved an extensive transfer of genes to the nuclear genome, resulting in a strong reliance on nuclear genes and cytoplasmic machinery for protein synthesis (Martin et al., 1998; Leister and Kleine, 2008). Thus, the envelope plays a primary role in the import of nuclear encoded chloroplast proteins (Soll and Schleiff, 2004). To facilitate crosstalk between the chloroplast and the cytosol, the envelope also harbours specific protein channels and transporters to facilitate the flux of ions and metabolites (Weber et al., 2005). While the IE typically comprises α-helical transport proteins, the OE is known to harbour a number of β-barrel channels, possibly being less substrate specific as compared to the IE (Schwenkert et al., 2023a; Schwenkert et al., 2023b). Notably, only very few proteins have been described to locate to the IMS, among them monogalactodiacylglycerol synthase 1 (MGD1) and the translocon of the chloroplast IE 22 (TIC22; Vojta et al., 2007).

Beyond these functions, the envelope is also one of the major sites for plant lipid metabolism, with chloroplast membranes accounting for 80% of glycerolipids in leaf mesophyll cells (Hölzl and Dörmann, 2019). This includes the shuttling of lipids and lipid precursors, as well as the biosynthesis of chloroplast specific lipids (Hölzl and Dörmann, 2019). Several envelope proteins have been associated with chloroplast lipid metabolism, such as the IE fatty acid exporter FAX1 (Li et al., 2015), the trigalactosyldiacylglycerol complex spanning both membranes (Fan et al., 2015) and the monogalactosyldiacylglycerol (MGDG) and digalactosyldiacylglycerol (DGDG) synthases (Shimojima et al., 1997; Dörmann et al., 1999; Awai et al., 2001; Kelly and

Dörmann, 2002), which are attached to the OE as well as the IE, with MGD1 facing the IMS.

The ability of plants to adjust to challenging environmental conditions is heavily dependent on changes in chloroplast metabolism. As a result, the import of nuclear encoded proteins as well as the shuttling of metabolites in and out of the chloroplast play a vital role in such acclimation processes (Eisa et al., 2020; Kleine et al., 2021; Schwenkert et al., 2022). Additionally, the chloroplast membranes undergo complex remodelling processes to maintain fluidity and stability under abiotic stress (Degenkolbe et al., 2012; Barrero-Sicilia et al., 2017; Li et al., 2020). Over the past years, proteins in the chloroplast envelope in particular have been increasingly recognised for their role in plant responses to cold stress (Trentmann et al., 2020; Schwenkert et al., 2023b; John et al., 2024).

Chloroplast Lipid Remodelling Protein 23 (CLRP23; At2g17695) was originally identified in chloroplast envelope membranes of *Pisum sativum* (Goetze et al., 2015). Due to the absence of a predicted transit peptide the protein was suggested to reside in the OE and named outer envelope protein (OEP23 – from here on named CLRP23). Its exact molecular mechanism, however, remains elusive. In this work, we aimed to investigate the molecular function of CLRP23 in Arabidopsis and explore its role in lipid remodelling during cold acclimation.

Results

CLRP23 shares structural similarities to the SRPBCC protein superfamily and is strongly anchored to the membrane.

To gain insight into the structure of CLRP23 and to identify conserved features, an *in silico* search using the template-based modelling software Phyre2.2 was performed (Powell et al., 2025). Intriguingly, high similarity to proteins of the SRPBCC (START/RHO_alpha_C/PITP/Bet_v1/CoxG/CalC) superfamily was found. The top three ranking protein templates for the structural prediction analysis are members of the STAR-related lipid transfer (START) domain protein family, which are known for their ability to bind hydrophobic ligands (Supplementary Fig. S1B; Radauer et al., 2008; Soccio & Breslow, 2003). Overall, 139 residues (with a coverage of 68%) were predicted with a confidence of 86.4% (Supplementary Fig. S1A). Structural prediction of CLRP23 in the AlphaFold Protein Structure Database (AlphaFold DB; Jumper et al.,

2021; Varadi et al., 2023) is highly similar to the model predicted by Phyre2.2 (Fig. 1A). Unlike the classical β-barrel protein channels and α-helical transport proteins typically found in the chloroplast envelopes, CLRP23 appears to have a mixture of both α-helixes and β-sheets in its predicted structure, with the β-sheets forming an incomplete β-barrel.

Next, we aimed to characterize the association of CLRP23 to the membrane. Isolated Arabidopsis membranes were treated with acidic or chaotropic reagents, total membrane and soluble fractions were obtained by centrifugation and analysed by SDS-PAGE and immunoblotting. CLRP23 did not dissociate from the membrane fraction in the presence of HCl, NaCl or urea, indicating a strong attachment to the membrane (Fig. 1B). Antisera against photosystem II extrinsic protein O (PsbO) and the translocon of the chloroplast IE 110 (TIC110) were used as markers for peripheral and integral membrane associations, respectively. Treatment with Lithium dodecyl sulfate (LDS) was used as a positive control and released all three proteins from the membrane as expected.

CLRP23 localizes to the chloroplast inner envelope facing the intermembrane space.

Although we could confirm a strong membrane association of CLRP23 with the membrane fraction, its localisation to the OE has yet to be experimentally confirmed. To investigate the localisation and topology of the protein in pea as well as in Arabidopsis, antisera against both proteins were generated. For subfractionation analysis, both Arabidopsis and pea chloroplasts were isolated and fractionated into stroma, thylakoid and envelopes. A highly pure separation of OE and IE membranes is only achievable in pea (Bölter et al., 2020), whereas in Arabidopsis only a mixed or enriched IE/OE fraction can be isolated. Accordingly, immunoblots were performed of isolated chloroplast stroma (Str), envelope (Env) and thylakoid (Thy) subfractions in Arabidopsis (Fig. 1C), as well as isolated chloroplast inner (IE) and outer (OE) envelope subfractions in pea (Fig. 1D). While we were able to confirm the localisation of CLRP23 to the Env subfraction in Arabidopsis, psCLRP23 could only be detected in the IE subfraction in pea, in contrast to the prior assumption (Goetze et al., 2015). Antisera against fructose-1,6-bisphosphatase (FBPase, Str), PsbO (Thy), TIC110 (Env), OE protein 37 (OEP37, OE), and the translocon of the chloroplast IE 40 (TIC40, IE) were used as markers for each subfraction.

To assess the purity of our OE and IE pea membranes, proteins of 5 (OE) and 6 (IE) biological replicates were analysed by mass spectrometry and quantified by label-free quantification (LFQ). In total 858 proteins were identified. To allow a better annotation of the proteins and connection to known functions and localisations all pea proteins were blasted against the Arabidopsis proteome. To identify Arabidopsis homologs, Arabidopsis gene IDs and their confirmed localisations are shown alongside the identified pea proteins in Supplementary Table S1. To assess the purity of the fractions, we compared the LFQ intensities of proteins found in the IE and OE fractions. A scatter plot of mean LFQ intensities (Fig. 1E) revealed a distinct separation between proteins annotated as IE and OE, indicating successful fractionation. Proteins associated with the IE exhibited systematically higher intensities in the IE fraction, while OE proteins were more abundant in the OE fraction, supporting the expected localization. Proteins clustering between the two groups likely represent contaminants from other chloroplast compartments. To show statistically significant differential enrichment of proteins in either fraction, a Student's t-test was performed and the $\log_2$ fold change was plotted against the $-\log_{10}$ p-value (Fig. 1F). Proteins assigned as IE or OE proteins are indicated. CLRP23 was clearly enriched in the IE fraction, with a $\log_2$ fold change of 2.04 when comparing IE vs. OE (Fig. 1F, Supplementary Table S1).

To further probe the localisation and topology of CLRP23, a "dual protease" approach was used. Intact chloroplasts of Arabidopsis were treated with increasing amounts of Trypsin or Thermolysin, followed by immunoblotting with antisera against CLRP23 (Fig. 1G). Under the proper reaction conditions, Thermolysin digests proteins facing the cytosol while leaving the OE intact, whereas Trypsin can partially disrupt the OE and thus digest proteins that are facing the intermembrane space (IMS) (Froehlich, 2011). CLRP23 was found to be digested by Trypsin, but not Thermolysin, thus suggesting that it is localised to the chloroplast IE facing the IMS (Fig. 1H). Antisera against TIC40 and TOC64 were used as markers for IE and OE proteins, respectively. Coomassie Brilliant Blue (CBB) was used as a loading control.

Loss of CLRP23 impairs photosynthetic performance under low-temperature stress.

To elucidate the molecular function of CLRP23, Arabidopsis knock-out mutants were generated using CRISPR-Cas technology and verified with Sanger sequencing to confirm homozygous gene disruption (Supplementary Fig. S2, S3A). One representative line was chosen for downstream experimentation and further verified

with immunoblotting of total protein extract to ensure the successful knock-out of CLRP23 (Fig. 2A).

In a previous proteomics study, CLRP23 was identified as differentially expressed in Arabidopsis chloroplast envelopes after cold treatments (Trentmann et al., 2020). This prompted us to investigate if *clrp23* mutants exhibit phenotypic alterations when subjected to low-temperature stress conditions. 20-day old plants grown under standard growth conditions (SGC) were subjected to six days cold treatment (4ºC, 250 µE, 16h light). While Col-0 typically starts to accumulate anthocyanins after several days of cold treatment, *clrp23* did not show this behaviour (Fig. 2B). To analyse the photosynthetic performance Chl *a* fluorescence parameters were measured, and *clrp23* showed a significant loss in PSII efficiency (Fv/Fm) after just one day of cold treatment (Fig. 2C). *Clrp23* also exhibited decreased PSII quantum yield (φ(PSII)), which was accompanied by decreased nonphotochemical quenching (φ(NPQ)) and increased nonregulated energy dissipation (φ(NO)), indicative of photosynthetic dysregulation and increased oxidative stress (Fig. 2D). After four days of cold treatment, Fv/Fm was drastically impaired in *clrp23*. Notably, photosynthetic parameters return to wild type-levels after recovery under SGC for five days. Cold-sensitivity in *clrp23* was not accompanied by noticeable effects on survival when subjected to freezing conditions (Supplemental Fig. S2B-C)

At low temperature, enzymatic activities in the chloroplast are limited while the light harvesting system remains unaffected. This imbalance can result in the generation of reactive oxygen species (ROS), thereby increasing the susceptibility of higher plants to light-induced damage (Miura and Furumoto, 2013). To separate the effects of light and cold, 20-day old plants were also treated with high light (22ºC day/18ºC night, 500 µE, 16 h light) and cold/low light (4ºC, 80 µE, 16 h light) (Supplementary Fig. S3D-G). *Clrp23* mutants showed a significant loss in Fv/Fm after both treatments. While Fv/Fm recovered to wild-type like levels after three days of high light treatment, Fv/Fm continued to decrease under cold/low light treatment, albeit to a lesser extent. This suggests that the loss of photosynthetic performance is primarily driven by low-temperature stress and exacerbated by increased light intensity.

To ensure the cold-sensitive phenotype observed was indeed caused by the disruption of *CLRP23*, complementation lines were generated by expressing *CLRP23* cDNA under the control of the 35S promoter in knockout mutants (Fig. 2A; Supplementary

Fig. S3A). The phenotype of the complemented mutants (*clrp23 com*) showed a complete recovery of photosynthetic parameters to wild-type-like levels under cold treatment (Fig. 2B-D).

Transcriptomic and proteomic responses of clrp23 *to low-temperature stress.*

To gain insight into the cellular pathways affected by the loss of CLRP23, we conducted transcriptomic (Supplementary Table S2) and proteomic (Supplementary Table S3) analyses comparing plants grown at SGC and plants after four days of cold treatment (4ºC, 250 µE, 16 h light). Differentially regulated genes (DEGs) and proteins (DEPs) after cold treatment vs SGC were identified by performing a Student's t-test for both Col-0 and *clrp23*, respectively. The results of the Student's t-tests are depicted in volcano plots (Fig. 3).

To assess the effect of cold treatment on Col-0 and *clrp23*, we used a list of cold regulated genes (CRGs) identified in a comprehensive meta-analysis of multiple studies (Hannah et al., 2005). These CRGs were found in the meta-analysis to be differentially expressed after at least 48 h of cold exposure. CRGs detected in the transcriptomic and proteomic datasets are highlighted in the volcano plots (green for upregulated genes and brown for downregulated genes), and the overlap between CRGs and the DEGs and DEPs identified in our analyses is depicted in Venn diagrams (Fig. 3A, C, E, G). Of the overlapping CRGs, 84% in the transcriptome and 91% in the proteome of Col-0 exhibited a similar response to cold treatment compared to SGC (Fig. 3A, C). Similarly, 77% of CRGs in the transcriptome and 84% in the proteome of *clrp23* exhibited a similar response to cold as compared to SGC (Fig. 3E, G). Although *clrp23* is cold-sensitive, its transcriptomic and proteomic responses to cold are consistent with published studies on transcriptomic response to long-term cold exposure in Arabidopsis. We therefore assume it is unlikely that this cold-sensitive phenotype stems from a disruption in cold stress signalling.

A similar approach was applied to a list of high light regulated genes (HRGs) identified in a meta-analysis of high light exposure (48-120 h; Bobrovskikh et al., 2022). HRGs detected in the transcriptomic and proteomic datasets are highlighted in a separate set of the same volcano plots (yellow for upregulated genes and blue for downregulated genes), and the overlap between HRGs and the identified DEGs and DEPs is shown in Venn diagrams (Fig. 3B, D, F, H). Among the HRGs overlapping with our analysis, only 38% and 34% of the transcriptome and proteome of Col-0 exhibited a similar

response under cold treatment (Fig. 3B, D). In *clrp23*, the percentages were 38% and 14%, respectively (Fig. 3F, H). These findings confirm that transcriptomic and proteomic responses to cold treatment in both Col-0 and *clrp23* appear to be primarily driven by cold.

Next, we examined the DEPs in the proteome of *clrp23* vs Col-0 under both SGC and after four days of cold treatment in more detail. While no significant alterations were observed in the proteome of *clrp23* under SGC (Fig. 4A), DEPs were identified after four days of cold treatment (Fig. 4B). Gene ontology (GO) term enrichment revealed a significant downregulation of proteins involved in flavonoid biosynthesis (Fig. 4B; Supplementary Table S4), including chalcone synthase (CHS), chalcone isomerase (CHI3), and flavanone 3-Hydroxylase (F3H), as well as enzymes acting further downstream in anthocyanin biosynthesis, including Dihydroflavonol 4-Reductase (DFR), Leucoanthocyanidin Dioxygenase (LDOX) and Anthocyanin 3-O-Glucoside Xylosyltransferase (A32gXYLT). To investigate this in more detail, anthocyanins were extracted and photometrically measured from both *clrp23* and Col-0 under SGC and after cold treatment. A reduction in anthocyanin accumulation was observed in *clrp23* after cold treatment compared to Col-0 (Fig. 4C).

Clrp23 *knockout mutants fail to accumulate neutral lipids and displays altered galactolipid remodelling under low temperature stress.*

Structural similarities between CLRP23 and the SRPBCC protein superfamily as shown earlier indicates the potential presence of a hydrophobic ligand binding domain. Since lipid remodelling under cold acclimation is known to play a role in maintaining membrane fluidity and influence cold signalling (Degenkolbe et al., 2012; Barrero-Sicilia et al., 2017), we investigated the effect of cold treatment on the lipid composition in *clrp23* (Supplementary Table S4). A liquid chromatography-mass spectrometry (LC-MS) based method was first used to determine the lipidomes of *clrp23* and Col-0 under SGC and after 4 days of cold treatment (Fig. 5A). This was complemented with gas chromatography-flame ionization detection (GC-FID) to analyse the fatty acid composition of total lipids, as well as MGDG and DGDG lipid fractions (Supplementary Fig. S4-5). Quantification of total lipids using GC-FID revealed no significant changes in total lipid content in *clrp23* and Col-0 under both SGC and after cold treatment (Fig. 5B). Z-score based k-means clustering analysis was used to group LC-MS quantified

lipid data into 5 clusters. While most lipid classes were distributed across multiple clusters, certain lipid classes showed distinct grouping patterns (Fig. 5A).

A large number of neutral lipids, namely two of the three diacylglycerol (DAG) species and all triacylglycerol (TAG) species were predominantly found in cluster 2 (Fig. 5A). To investigate this further, the relative abundance values of all neutral lipid species (DAGs and TAGs) quantified with LC-MS were summed and normalised to Col-0 levels under SGC. On average, cold treatment induced an approximate 3.6-fold increase in neutral lipids in Col-0, an effect that was not observed in *clrp23* (Fig. 5F). The accumulation of neutral lipids in Arabidopsis during cold acclimation has previously been reported and is speculated to result from the storage of excess fixed carbon as growth is arrested under low temperature conditions (Degenkolbe et al., 2012). However, neutral lipids can also accumulate due to adjustments in membrane fluidity and stability as part of the cold acclimation program. In particular, DAGs, which are later converted to TAGs, can be synthesised from MGDG by SENSITIVE TO FREEZING 2 (SFR2) under freezing conditions (Moellering et al., 2010). To ensure the lack of neutral lipid accumulation observed in *clrp23* under cold is not related to the SFR2 pathway, LC-MS lipid quantification was also performed on plants undergoing freezing recovery (Supplementary Table S5). Neutral lipids in *clrp23* accumulated to wild-type-like levels after 1 hour of freezing recovery (Fig. 5G), suggesting that the lack of neutral lipid accumulation after cold treatment is due to the lack of fixed carbon resulting from impaired photosynthesis.

Six of the eight MGDG species grouped in cluster 1, where their levels decreased in Col-0 after cold treatment – an effect that appears to be even more pronounced in *clrp23* (Fig. 5A). The contrasting response of these MGDG species, compared to the highly unsaturated 34:6 and 36:6 species found in cluster 4, prompted us to further examine overall MGDG saturation levels. To assess this, the double bond index (DBI), calculated as Σ (% lipid or fatty acid × number of double bonds) was determined for all MGDG lipid species quantified with LC-MS (Fig. 5D), and for all MGDG fatty acids quantified with GC-FID (Fig. 5E). Cold treatment increased the DBI of MGDG lipids in Col-0, with an even greater increase in *clrp23* (Fig. 5D). A similar trend was observed in the DBI of MGDG fatty acids, where only *clrp23* showed a significant increase after cold treatment (Fig. 5E).

MGDG is a non-bilayer forming lipid, with the tendency to form inverted hexagonal (H_{II}) phases (Fig. 5H; (Webb and Green, 1991). A reduction in MGDG/DGDG ratio was observed in Col-0 after cold treatment, with an even greater reduction observed in *clrp23* (Fig. 5C). This, along with the increased desaturation of MGDG lipids following cold treatment, indicates a more pronounced galactolipid remodelling response in *clrp23* under low-temperature stress.

CLRP23 binds to chloroplast membrane lipids in silico.

Molecular docking simulations were conducted to explore potential interactions between CLRP23 and chloroplast membrane lipids. Using Autodock 4.2 (Morris et al., 2009), the 3D structure of CLRP23 was docked against MGDG, DGDG, SQDG and PC (Fig. 6). CLRP23 showed the strongest binding affinity for MGDG (-6.7 kcal/mol), and weaker binding affinities for DGDG (-4.6 kcal/mol) and SQDG (-4.3 kcal/mol). Although CLRP23 also showed a relatively strong binding affinity for PC (-6.4 kcal/mol), it is noteworthy that PC is a chloroplast membrane lipid that is only found on the outer leaflet of the OE. Given CLRP23's localisation to the IE and orientation to the IMS, it is unlikely for CLRP23 to interact with PC in vivo. While all lipid ligands dock to the same hydrophobic binding pocket in the protein, the hydrophilic heads of PC and MGDG are oriented inside of the pocket, while the heads of DGDG and SQDG face outwards. A distance-based approach (<3.5Å) identified 17 amino acid residues that come into contact with at least one of the lipids in the docking simulations (Fig. 7).

To assess the conservation of these residues across species, we investigated the phylogenetic background of CLRP23. A sequence-based search for the top 100 homologs was performed against streptophytes, chlorophytes as well as the NCBI database excluding Viridiplantae (e-value $<10^{-7}$, Supplementary Table S6). A phylogenetic analysis revealed two distinct clades: one comprising the Chloroplastida, the other consisting of prokaryotic sequences (Supplementary Figure 6). To further explore the evolutionary distribution, we searched the NCBI database for Rhodophythes, Glaucophytes and Cyanobacteria. In addition, a search excluding Viridiplantae and bacteria was performed. These searches retrieved homologous sequences from Chlorophytes, Haptophytes and Amorphaea, as well as from archaea and a limited number of cyanobacteria (Supplementary Table 6). However, homologs in Asgard archaea, the lineage that gave rise to eukaryotes (Eme et al., 2023) were not found. Next, a structure-based search was performed. With this approach,

homologues were mainly retrieved from bacteria (pLDDT≥70, Supplementary Table 6, Supplementary Figure 7). Beyond the sequence-based approach, we observed a broader distribution of eukaryotic homologs, including a few Asgard archaea with a conserved core. Together, these findings suggest that the CLRP23 gene family may be ancient, although restricted to specific eukaryotic groups, a few archaea and some cyanobacteria.

Next, we aligned closely related CLRP23 orthologs from nine land plant species, spanning dicots, monocots, lycophytes, and bryophytes, to examine lipid-interacting residues in detail. (Fig. 7). Four residues (H143, E148, L175 and F190) are fully conserved among the 9 homologs we analysed. Other residues that are less well conserved often saw amino acid substitutions with similar properties. One residue of particular interest was F190, which was only identified as a contact site in the docking simulation with MGDG. F190 also had the shortest distance to the ligand (2.5 Å) and is fully conserved among the putative orthologs analysed. These data suggest that the CLRP23 family is not only traceable to the last common ancestor of land plants but that also its lipid-interaction is conserved across land plants.

Discussion

Prior to this study, psCLRP23/OEP23 had been described as a protein channel based on electrophysiological measurements suggesting cation-selective activities *in vitro* (Goetze et al., 2015). Due to the absence of a predicted transit peptide, the protein was assumed to localise to the OE, since these proteins typically lack classical transit peptides (Kim et al., 2019). However, the localisation of CLRP23 to the OE has not been experimentally demonstrated. In this study, we provide evidence that CLRP23 localises to the IE, facing the IMS, and explore its molecular role in lipid remodelling during cold acclimation.

Based on structural predictions using AlphaFold2 and Phyre2, CLRP23 consists of a mixture of both α-helical and β-sheet structures resulting in the formation of an incomplete β-barrel. We also observed a high degree of structural similarity between CLRP23 and proteins in the SRPBCC superfamily, a protein superfamily characterized by a common 3-dimensional structure, albeit similarities on the sequence level are often less pronounced. Proteins of the superfamily typically comprise a large hydrophobic binding cavity for ligands such as membrane lipids, secondary

metabolites, polycyclic aromatic hydrocarbons, and plant hormones (Radauer et al., 2008). Our subfractionation analysis very clearly showed an enrichment of CLRP23 in the chloroplast IE, rather than OE. Combined with protease treatments, our findings show that CLRP23, despite being strongly anchored to the membrane, is rather a peripheral membrane protein on the chloroplast IE, with a significant portion of the protein facing the IMS. Although the mechanism by which CLRP23 is targeted to the IMS without a predicted transit peptide remains to be elucidated in the future, the structural predictions, along with our experimental evidence, suggest an alternative role for CLRBP23, differing from its previously proposed function as an OE channel.

This alternative molecular role of CLRP23 was further explored by generating knock-out lines. Arabidopsis mutants deficient in CLRP23 suffer from impaired photosynthesis and reduced anthocyanin accumulation after several days of cold treatment. The cold-sensitive phenotype observed in *clrp23* adds to the growing body of evidence linking chloroplast envelope membrane proteins to plant acclimation (Trentmann et al., 2020; Schwenkert et al., 2023b; John et al., 2024).

Anthocyanins are a major class of flavonoids, a group of secondary metabolites characterised by their polyphenolic three-ring chemical structure (Petrussa et al., 2013). Flavonoids are primarily synthesised from photosynthetically derived carbon along the Phenylpropanoid pathway and are well known to be involved in a wide variety of plant abiotic stress responses (Di Ferdinando et al., 2012; Petrussa et al., 2013; Shomali et al., 2022; Kitashova et al., 2023; Kitashova et al., 2024). During cold acclimation in particular, flavonoids accumulate after several days and have been shown to play a role in balancing C/N metabolism and maintaining protein homeostasis (Kitashova et al., 2024). However, unlike *clrp23*, photosynthesis of mutants deficient in flavonoid biosynthesis decrease in a similar manner during cold acclimation compared to Col-0 (Kitashova et al., 2023). The downregulation of flavonoid metabolism is therefore unlikely to be the sole cause of the cold-sensitive phenotype observed in *clrp23*.

Conversely, it has been shown that Arabidopsis mutants suffering from impaired photosynthesis also exhibit deficiencies in the synthesis and accumulation of flavonoids (Vicente et al., 2023; Scherer et al., 2024). Thus, it is more likely that the reduced flavonoid biosynthesis and anthocyanin accumulation observed in *clrp23* mutants under cold conditions are due to a lack of fixed carbon resulting from impaired

photosynthesis. Consistent with this, triacylglycerols also fail to accumulate in *clrp23* under cold conditions, suggesting a broader disruption in carbon allocation.

Beyond flavonoid metabolism, lipid remodelling is another key aspect of cold acclimation and is crucial for preserving membrane fluidity and structural integrity. The primary chloroplast membrane lipids, galactolipids MGDG and DGDG, undergo structural and compositional modifications in response to low temperatures (Degenkolbe et al., 2012; Barrero-Sicilia et al., 2017; Li et al., 2020). To counteract the rigidifying effects of low temperature, membrane lipids undergo an increase in fatty acid desaturation, introducing double bonds that create conformational kinks in lipid hydrocarbon chains. These structural changes reduce intermolecular packing and thereby enhance membrane fluidity (Hugly and Somerville, 1992; Murakami et al., 2000; Routaboul et al., 2000). In addition, MGDG is a non-bilayer forming lipid that is conical in shape with a tendency to form hexagonal HII phases (Webb and Green, 1991). To maintain membrane integrity and stability, plants also reduce the ratio of non-bilayer to bilayer forming lipids such as MGDG/DGDG as an adaptive strategy to a variety of environmental stresses, including low temperature stress (Moellering et al., 2010; Zheng et al., 2016; Li et al., 2020; MacDonald et al., 2023).

Intriguingly, *clrp23* exhibited an exaggerated MGDG fatty acid desaturation as well as a more pronounced decrease in MGDG/DGDG ratio as compared to Col-0 after cold treatment, strongly suggesting an imbalance in lipid remodelling on various levels during cold acclimation.

Lipid remodelling is highly complex, and involves the intricate balance between membrane fluidity, stability and functionality. While the biophysical characteristics of lipid desaturation is essential for cold acclimation, studies have demonstrated that other factors such as lipid shape also play a major role (Barkan et al., 2006; Degenkolbe et al., 2012). Saturated species of MGDG are predicted to be narrower than their more unsaturated counterparts (Gounaris et al., 1983; Gruner et al., 1985) and increases in MGDG saturation has also been postulated to help stabilise the membrane against the formation of H_{II} phases (Degenkolbe et al., 2012). A lipidomics study of 15 different Arabidopsis accessions found that the more saturated MGDG species 34:2 and 34:3 correlated positively with acclimated freezing tolerance (Degenkolbe et al., 2012). Hence, MGDG desaturation beyond what is required for

membrane fluidity, such as that observed in *clrp23* under cold treatment, may have detrimental effects on membrane stability.

Furthermore, MGDG lipids make up 50% of the lipids present in the thylakoid membrane and, along with other thylakoid lipids, are integral to the assembly and function of photosynthetic complexes (Hölzl and Dörmann, 2019; Yoshihara and Kobayashi, 2022). In particular, the conical shape of MGDG has been found to sterically complement the hourglass shape of trimeric Light-harvesting complex II (LHCII), stabilising it against unfolding (Seiwert et al., 2017). While the reduction of MGDG/DGDG ratio is a well-documented adaptive strategy against abiotic stress, Arabidopsis maintains a higher ratio than rice plants despite being more tolerant to low temperatures (Zheng et al., 2016), suggesting that the ability of plants to modulate this ratio is more crucial than its absolute value. We therefore suggest that the excessive reduction of MGDG/DGDG ratio, combined with an excessive increase in MGDG desaturation observed in *clrp23* under cold, may destabilise the membrane and alter packing relationships between membrane lipids and photosynthetic complexes, ultimately disrupting lipid-protein interactions crucial for photosynthetic function.

Changes in the lipidome, as well as the structural similarities between CLRP23 and the SRPBCC superfamily suggest a direct interaction of CLRP23 and chloroplast lipids. Indeed, in silico docking simulations of CLRP23 revealed an affinity for chloroplast membrane lipids, with the strongest binding observed for MGDG. The residue F190, which showed the shortest ligand distance and was found to dock exclusively with MGDG, was completely conserved in all orthologs of CLRP23 in our sequence alignment analysis, emphasising a potential occurrence of CLRP23-MGDG interaction *in vivo*. Strikingly, CLRP23 is one of the very few chloroplast envelope proteins currently known to face the IMS. One of the few other characterized IMS proteins is MGD1, the major chloroplast MGDG synthase (Vojta et al., 2007). This raises the question of whether CLRP23 works in concert with MGD1 to fine-tune galactolipid remodelling during cold acclimation, a question that should be addressed in future studies.

Our finding that CLRP23 likely has an ancient origin aligns with its role in lipid remodelling, a fundamental process in all organisms. Interestingly, it has been speculated, that the eukaryotic endomembrane system originated from bacterial outer membrane vesicles (Gould et al., 2016). Our docking analysis suggests a potential

binding to PC in addition to or as an alternative to galactolipids, raising the possibility for a similar function of its non-galactolipid containing relatives. The absence of sequence homologs in Asgard archaea, suggests either early acquisition via endosymbiotic gene transfer followed by losses, or lateral gene transfer among prokaryotes with subsequent transfers into eukaryotes. This is consistent with the observations that (i) the top100 homologs to Arabidopsis CLRP23 are exclusively bacterial when searching in all datasets except Viridiplantae and (ii) bacterial homologues are predominantly recovered by structure-similarity based searches. Distinguishing between the two outlined scenarios is challenging due to the recurrent lateral gene transfers among prokaryotes. However, this could be addressed by a combined sequence- and structure-based phylogenetic approach in the future.

Unfortunately, attempts to express and purify soluble and correctly folded CLRP23 in *E. coli* with sufficient yield, stability and purity for downstream interaction assays have thus far been unsuccessful. Presumably, tagging of the C- or N-terminus of the protein disrupts its structural integrity and functionality, calling for more sophisticated approaches for future *in vitro* studies to investigate binding of lipids or other proteins to CLRP23.

Together, our findings indicate that CLRP23 is involved in modulating MGDG dynamics, a crucial aspect of lipid remodelling to maintain chloroplast membrane stability and function during cold acclimation. We hypothesize that its mode of action is closely linked to the activity of MGDG synthase in the IMS, where CLRP23 may function as an MGDG-binding scaffold protein during lipid remodelling under cold acclimation.

Material and Methods

Plant material and growth conditions

CRISPR/Cas9 mutants of *CLRP23* were generated in Arabidopsis Col-0 background. Specific guide RNAs in the 2nd exon were designed using the web server https://chopchop.cbu.uib.no/ (5’-AGTACAGAGGAGTTTCGTCT-3'; 5’-TGGTAGAGAGAGTTATGAGA-3'). Guide RNAs were cloned into lvl0 vectors resulting in ProU6 driven expression units. Using GoldenGate cloning, these lvl1 guide RNA containing vectors were assembled with a ProRPS5a driven multi-intron CAS9 (Grützner et al., 2021) and a fluorescent seed coat transformation marker (Shimada et

al., 2010) into a binary plant expression vector. Arabidopsis plants were transformed using *Agrobacterium* strain GV3101 by the flower dip method (Clough and Bent, 1998). Transformed seeds were selected using the fluorescence marker. In the second-generation, knock-out mutants free of the CAS9 construct were selected by screening for non-fluorescent seeds (Ursache et al., 2021). Successful knockdown of CLRP23 was verified via immunoblotting and PCR genotyping (5'-TCACGAAGCATTGACATGTTTCA-3', 5'-ATGGTGTTCTTGAGTTGGGG-3'). PCR genotyping was performed by amplifying *CLRP23* from extracted genomic DNA (Kotchoni and Gachomo, 2009) with Taq-polymerase PCR. PCR products were sequenced with Sanger Sequencing (LMU Faculty of Biology, Genetics Sequencing Service).

To complement the *clrp23* mutant the coding sequence of *CLRP23* including a stop codon was cloned into pB7FWG2 (Karimi et al., 2002) using Gateway cloning. *Clrp23* mutants were transformed with Agrobacteria strain GV3101 carrying the respective construct by the flower dip method (Clough and Bent, 1998). Transformed plants were selected by treatment with glufosinate-ammonium (BASTA). Successful knockdown of CLRP23 was verified via immunoblotting and PCR genotyping using primers specific for genomic *CLRP23* (5'-TCCTTCCCTTTCATCTTCATTTTTGG-3', 5'-TGCAGGTTCTTCTTCTCTCTACAC-3').

Arabidopsis plants were grown on soil in a growth chamber under long-day conditions [16 h/8 h day-night cycle, 120 µE $m^{-2}s^{-1}$, temperatures 21°C/ 18°C (light/dark)] for three weeks. For cold and light treatments plants were grown at the indicated conditions. Pea plants (*P. sativum* L., cv. 'Arvica', Prague, Czech Republic) were grown on vermiculite for 10 days in a climate chamber [14 h/10 h day-night cycle, 120 µE $m^{-2}s^{-1}$, temperatures 20°C/ 14°C (light/dark)].

Freezing treatment of Arabidopsis was performed according to Trentmann et al. (2020) with small changes. Four-week-old plants were cold acclimated for four days under short day conditions (light 10 h/4°C; dark 14 h/4°C). At the following day, the diurnal cycle was turned off and the temperature was gradually lowered from 4°C to -10°C, with a stepwise temperature decrease of 2 to 4°C per h. The freezing temperature of -10°C was kept constant for 15 h, after which the temperature was raised again to 22°C, with a stepwise temperature increase of 2 to 4°C/h. The diurnal cycle was turned on again after one day, when the temperature was recovered back to 22°C (light

10 h/22°C; dark 14 h/18°C). Two rounds of freezing experiments were performed on a combined total of 110 Col-0 and *clrp23* mutant plants each. After freezing, samples were collected for lipidomic analysis after temperatures were recovered for 1 h at 22ºC.

Immunoblot analysis

SDS-polyacrylamide gel electrophoresis (PAGE) was performed as described by Laemmli (Laemmli, 1970). Proteins, separated via SDS-PAGE, were transferred onto PVDF membranes (Immobilon-P, Millipore, Darmstadt, Germany) via semi-dry blotting.

For CLRP23 antibody generation the coding sequence of *CLRP23* and *psCLRP23* were cloned into pET51b$^+$, both proteins were purified from inclusion bodies and antisera were generated (Biogenes, Berlin, Germany).

Arabidopsis chloroplast isolation, subfractionation and protease treatment

Arabidopsis chloroplasts and envelopes were isolated according to Dischinger and Schwenkert (2022). For CLPR23 membrane extraction Arabidopsis leaves were homogenised in wash buffer (100 mM Sucrose, 10 mM HEPES-NaOH pH 8), filtered and centrifuged for 10 min at 10.000 *g* and 4ºC. The pellet fraction was treated either with buffer (100 mM Sucrose, 10 mM HEPES-NaOH, pH 8) or different chaotropic reagents (final concentration of 1 M NaCl, 0.1 M HCl, 4 M urea or 2% LDS, respectively). Samples were incubated for 30 min on ice and centrifuged for 10 min at 10.000 x *g* and 4ºC to separate the soluble and membrane fraction before subjection to SDS-PAGE and immunoblotting.

For protease treatment, chloroplasts equivalent to 100 µg of chlorophyll were pelleted and resuspended in 100 µl of wash buffer supplemented with 0.5 mM $CaCl_2$. Trypsin or Thermolysin was added at the specified amounts per mg of chlorophyll, and the mixture was incubated at 23 °C for 40 min. To stop the reaction, 1× complete protease inhibitor (CPI) was added. Chloroplasts were then re-isolated by centrifugation and washed once with wash buffer containing 1× CPI. The final pellet was solubilized in Laemmli loading buffer supplemented with 2 M urea and 1× CPI, heated at 65 °C for 5 min, and chloroplasts equivalent to 15 µg of chlorophyll were loaded onto an SDS-PAGE gel. Immunoblotting was performed as described above.

Chlorophyll fluorescence measurements

The photosynthetic activity of PSII was assessed by measuring chlorophyll *a* fluorescence using the HEXAGON-IMAGING-PAM system (Walz, Effeltrich,

Germany). Photosynthetic parameters were calculated using IMAGING-PAM software based on the equations described by Klughammer and Schreiber (2008). Three biological replicates, two leaves each, for each genotype and condition were measured.

Extraction and measurement of Anthocyanins

Anthocyanins were extracted and measured (four biological replicates) using a method described in Kitashova et al. (2023). In short, plant material was frozen and ground in liquid nitrogen before being suspended in 1M HCl and incubated at 25ºC for 30 min on shake (800 rpm). Samples were then centrifuged at 21,000 g for 10 min, and the supernatant was collected before the extraction was repeated once more at 80ºC for 30 min. After a second centrifugation step, the supernatant was collected and pooled for photometric quantification at 540 nm. Absorbance was normalised to fresh weight.

RNA sequencing and data analysis

Total RNA was extracted from plants using TRIzol (Invitrogen, Carlsbad, USA) and purified with Direct-zol™ RNA MiniPrep Plus columns (Zymo Research, Irvine, USA) following the manufacturer's instructions. RNA integrity and quality were assessed using an Agilent 2100 Bioanalyzer (Agilent, Santa Clara, USA). For RNA sequencing, ribosomal RNA was depleted to generate long non-coding RNA sequencing (lncRNA-seq) libraries, capturing both nuclear and organellar transcripts. Directional lncRNA-seq libraries were prepared, and 150 bp paired-end sequencing was performed at a depth of approximately 6 G on an Illumina NovaSeq 6000 system (Illumina, San Diego, USA) at Biomarker Technologies (BMK) GmbH (Münster, Germany) following standard Illumina protocols. Three independent biological replicates were analysed per genotype. RNA-Seq reads were processed using the Galaxy platform (Jalili et al., 2020) as described by Tang et al. (2024), with one modification: differential gene expression of both plastid- and nuclear-encoded genes was determined using DESeq2 (Love et al., 2014) with fit type set to "parametric," multi-mapping allowed, a linear two-fold change cutoff, and an adjusted P-value of < 0.05. One replicate of the *clrp23* mutant grown at room temperature was excluded as an outlier.

Lipidome analysis

Lipids and free fatty acids were extracted following the method described by Hummel et al. (2011). Briefly, 50 mg of each sample was extracted with 1 ml of a pre-chilled methanol:methyl tert-butyl ether (MTBE) solution (1:1, v/v) at −20°C. Internal standards

were added to the extraction mixture, including 2 µg ml-1 corticosterone, 0.25 µg ml-1 ampicillin, and 1 µg ml-1 chloramphenicol. Samples were shaken for 10 min at 4°C and then ultrasonicated for an additional 10 min on ice. Subsequently, 500 µl of water:methanol (3:1) was added to the mixture, which was vortexed for 10 sec and centrifuged at maximum speed for 5 min at 4°C. Phase separation resulted in an upper organic phase containing lipids and a lower phase containing polar and semi-polar metabolites. The upper organic phase (500 µl) was collected, dried under vacuum under argon gas, and stored at −80°C until further analysis.

For LC-MS analysis, a Dionex Ultimate 3000 UHPLC system (Thermo Fisher Scientific) coupled with a timsTOF mass spectrometer (Bruker Daltonik) was employed. The dried extracts were reconstituted in 100 µl of acetonitrile:isopropanol (7:3) and 5 µl was injected onto a C8 reversed-phase column (Ultra C8, 100 × 2.1 mm; Restek) with a flow rate of 300 µl min-1 at 60°C. The mobile phases were (A) water and (B) acetonitrile:isopropanol (7:3), both containing 1% (v/v) ammonium acetate and 0.1% (v/v) acetic acid. A 26 min gradient was used, beginning at 55% B and increasing to 99% B over 15 min. This was followed by a 5 min washing step at 99% B and a return to 55% B with a 5 min equilibration phase.

For mass spectrometry, an electrospray ionization (ESI) source operated in positive mode was utilized. Nitrogen was used as the dry gas at a flow rate of 8 l min^{-1}, a pressure of 8 bar, and a temperature of 200°C. Mass spectra were recorded in MS mode with a range of 50–1300 m/z, a resolution of 40,000, a scan speed of 1 Hz, and a mass accuracy of 0.3 ppm. Compounds were annotated using a targeted approach based on specific m/z values at defined retention times and their isotopic patterns. Data acquisition was performed using otofControl 6.2, with further analysis conducted using DataAnalysis 5.3 and MetaboScape 2021 software. Quantification was normalized to fresh weight and internal standards, excluding features detected in blanks or wash samples with a threshold of >10%. Three independent biological replicates were measured per genotype/condition for cold treatment, four for freezing recovery. For freezing recovery, one replicate of the *clrp23* mutant grown at room temperature was excluded due to technical reasons and was replaced by taking the average value of the remaining replicates.

Analysis of fatty acid composition

Lipids were extracted for Thin-Layer Chromatography (TLC) and fatty acid methyl ester (FAME) analysis using a method adapted from Yu et al. (2020). 500 mg of frozen and ground plant material was ground in liquid nitrogen and suspended in 6 ml CHCl3:MeOH (1:2 v/v), with 50 µl of 5 mg ml^{-1} tripentadecanoin (TAG C15:0) added to each sample as an internal standard. Cellular debris were removed by centrifugation at 2100 *g*, 4ºC for 5 min. 2 ml of CHCl3 and 1.2 ml of KCl (0.45 % v/v) was added to the resulting supernatant for phrase separation, and the lower green organic phase was collected. The solvent was evaporated by nitrogen stream and the lipids were resuspended in 250 µl CHCl3:MeOH (9:1 v/v).

For TLC, lipid samples were applied to a silica gel coated glass plate (20 x 20 cm) using an automatic TLC sampler (CAMAG® ATS 4). For each sample, a total of 8 µl of lipids were separated with acetone:toluene:water (91:30:8, v/v/v) and visualised with 0.05% primuline in acetone:water (8:2 v/v) under UV light (Hölzl and Dörmann, 2021). 4 µl each of MGDG and DGDG (2.5 mg/ml, Avanti Polar Lipids, Inc.) were also applied to the plate as external standards. Water was applied to MGDG and DGDG bands to prevent particle formation, and the silica was scraped with a spatula into a fresh glass tube. The silica containing MGDG or DGDG was then suspended in 0.5 ml anhydrous methanol and sonicated for 5 min, before evaporating the methanol by nitrogen stream.

Fatty acid methyl esters (FAMEs) were generated as described in Pålsson et al. (2024), slightly modified from (Leonova et al., 2008). In short, 2 ml of MeOH:H2SO4 (98:2 v/v) was added to either 8 µl lipid extract (for total lipid analysis) or dried silica from the previous TLC step (for MGDG and DGDG analysis). 10 µl of 0.25 mg ml^{-1} heptadecanoic acid (C17:0) was also added as an internal standard for the methylation reaction. Samples were methylated in a heat block at 80ºC for 45 min, after which 2 ml of water and 2 ml heptane was added for phase separation. The upper heptane phase was collected and evaporated under nitrogen gas and the FAMEs were resuspended in 50 µl cyclohexane.

The resulting FAMEs from the methylation step were then analysed on a Trace 1300 gas-chromatography (GC) machine equipped with an ISQ single quadrupole mass spectrometer (MS), a flame ionisation detector (FID) and an auto-sampler (Thermo Scientific). FAMEs were separated on a Zebron ZB-FAME column (20m x 0.18mm i.d. x 0.15 µm film thickness). The GC oven was set to a starting temperature of 90ºC,

which was held for 1.5 min before ramping at 5.5ºC/min to 240ºC. The oven was held at 240ºC for 4 min until the end of the program, with a total run time of 33 min. The MS was set with an MS line temperature and ion source temperature of 250ºC, and a full scan was performed with mass range of 50-500 amu and dwell time of 0.2 seconds. FAMEs were identified based on the retention time compared with the external reference standard GLC 426 (Nu-Check-Prep) and further confirmed with MS spectra using GC-MS, after which FID was then employed for the quantification of each FAME. The FID was set to a detection temperature of 260ºC. Chromeleon 7.3.1.6535 (Thermo Scientific) was used for data processing.

GLC 426 standard mix was used as the external standard to both identify the retention time and calculate the response factor for each FAME. The response factor, which accounts for the difference in detector response of each fatty acid (FA) compared to the internal standard C17:0 (IS), was calculated as follows:

$$D_{FA} = R_{FA}/R_{IS} = (A_{FA}/W_{FA})/(A_{IS}/W_{IS})$$

D = response factor; R = response; A = peak area (pA*min); W = weight. The response factor of C:17 was set to 1.

After subtracting the peak areas detected in the reaction blanks, the peak areas of each FAME were normalized according to the response factor of each FAME. For FAMEs C16:2 and C16:3, which were not included in the external standard, the response factor for the C16:1 FA was used for normalization. The final quantification of each FAME is reported as mol%. Total lipid content was calculated based on the sum of the normalized peak areas of all FAMEs, relative to the normalized peak area of the TAG IS C15:0, which was added as tripentadecanoin (Larodan, Sweden) to each sample prior to lipid extraction. Four independent biological replicates were used per genotype/condition for all measurements.

LC-MS/MS protein analysis

For Arabidopsis shotgun proteomics total proteins were extracted from 3-week-old rosette leaves by grinding frozen plant material in liquid nitrogen. A 100 mg aliquot of the resulting powder was suspended in 0.3 ml of extraction buffer (100 mM HEPES pH 7.5, 150 mM NaCl, 10 mM DTT, 6 M Guanidine Chloride, and Roche complete™ Protease Inhibitor Cocktail). The suspension was sonicated using a Branson Sonifier B-12 (Branson Ultrasonics, Danbury, USA) for three 20-second cycles and then incubated at 60°C for 10 min. Cellular debris was removed by centrifugation at 10,000

g for 15 min. Proteins were precipitated using the chloroform-methanol method. To the clarified supernatant, methanol, chloroform, and water were added in a 4:2:3 ratio. The mixture was centrifuged at 10,000 *g* for 10 min, and the protein interphase was collected and washed five times with methanol. The resulting protein pellet was dried and dissolved in 3 M Urea/2 M Thiourea in 50 mM HEPES (pH 7.8). Protein concentration was quantified using the Pierce 660 nm Protein Assay Kit (Thermo Fisher Scientific). For digestion, 100 µg of protein was reduced with 10 mM DTT for 30 min at 37°C, alkylated with 50 mM iodoacetamide (IAA) for 20 min at room temperature in darkness, and then digested overnight with 1 µg Trypsin (Thermo Fisher Scientific) at 37°C.

For envelope proteomics, chloroplasts were isolated from the leaves of 10-day-old pea plants and fractionated into IE and OE as described previously (Waegemann et al., 1992). IE and OE membrane samples (30 µg protein) were resuspended in 250 µl of extraction buffer, sonicated, incubated at 60°C, and centrifuged as described for plant powder. Protein digestion followed the FASP method (Wiśniewski et al., 2009). All digested peptides were purified using homemade C18 stage tips (Rappsilber et al., 2003).

For LC-MS/MS analysis, 1 µg of peptides was separated using a nano-LC system (Ultimate 3000 RSLC, Thermo Fisher Scientific) with linear gradients of 5% to 80% ACN (v/v) at a flow rate of 250 nl/min. Gradient lengths varied by sample complexity: 90 min for total proteins and 60 min for envelope samples. Chromatography was performed with Acclaim Pepmap nano-trap (C18, 100 Å, 100 µm × 2 cm) and analytical (C18, 100 Å, 75 µm × 50 cm) columns, with the column temperature maintained at 50°C. MS/MS was conducted on an Impact II high-resolution Q-TOF mass spectrometer (Bruker Daltonics, Bremen, Germany) using CaptiveSpray nano-electrospray ionization. MS1 spectra (m/z 200–2000) were acquired at 3 Hz, and the 18 most intense peaks were subjected to MS/MS at 4–16 Hz based on intensity. A dynamic exclusion duration of 0.5 min was applied.

Raw data were processed using MaxQuant (version 2.4.4.0) with peak lists matched against the Arabidopsis or *Pisum sativum* reference proteome (UniProt) using default parameters. Protein quantification was performed using the LFQ algorithm. Data were further analysed using Perseus (version 2.0.6.0). Contaminants, reverse hits, and proteins identified only by site modification were excluded. For *clrp23* proteomics

proteins quantified in at least three out of four replicates were retained. For envelope proteomics proteins quantified in at least four replicates were retained. LFQ intensities were log_2-transformed, and missing values were imputed using a normal distribution in Perseus. The Database for Annotation, Visualization, and Integrated Discovery (DAVID) was used to identify enriched gene ontology (GO) terms based on biological process (Huang et al., 2009; Sherman et al., 2022).

Molecular docking analysis

The 3D structure of At2g17695 (CLRP23) was downloaded in PDB format (UPF0548) from the AlphaFold Protein Structure Database (Jumper et al., 2021; Varadi et al., 2022). Using AutoDock 4.2 (Morris et al., 2009), the PDB files were prepared via removing water molecules, repair missing atoms, adding polar hydrogens, adding Kollman charges (Singh and Kollman, 1984), and checking total charges on residues. Several ligands were used for docking analysis, i.e., MGDG (CID: 5771744), DGDG (CID: 363608285), PC (CID: 52923341), and SQDG (CID: 363648189). The 3D conformation of the different ligands was either obtained as SDF files from the PubChem database (Kim et al., 2025) or generated based on the 2D conformations SDF files using OpenBabel v3.1.1 (O'Boyle et al., 2011). SDF files were then converted into PDBQT format in the AutoDock 4.2.

All the docking simulations performed in the current study were via AutoDock 4.2 and AutoDock Vina 1.2.0 (Trott and Olson, 2010; Eberhardt et al., 2021). Default docking parameters were chosen with a globally searching exhaustiveness of 8. The docking grid size was set to 44 × 64 ×58 Å where its centre corresponding to the centre of the receptor protein. The docking conformation with the lowest binding affinity (kcal mol-1) was adopted. Molecular graphing software ChimeraX-1.8 (Pettersen et al., 2004) and PyMOL (Schrodinger, 2010) were used for further visualisation and identification of contact sites.

Sequence homology and phylogenetic analysis

The Arabidopsis CLRP23 sequence was used to query our database of land plants and streptophyte and chlorophyte algae using BLASTp (references for the sequence databases are provided in Supplementary Methods S1). The results were filtered based on e-value and hits with an e-value of $\leq 10^{-7}$ retained. Additionally, we queried the nr database with the following restriction (i) excluding Viridiplantae, (ii) excluding Viridiplantae and bacteria, (iii) Cyanobacteria, (iv) Rhodophyta and (v) Glaucophyta

using an e-value cutoff of ≤10^{-7}. For phylogenetic analysis the BLASTp output was aligned using MAFFT with G-INS-I (Katoh and Standley, 2013). After a quality control a maximum likelihood phylogeny was constructed using IQTree with 100 bootstraps per phylogeny (Nguyen et al., 2015). The model was selected using modelfinder implemented in the software (Kalyaanamoorthy et al., 2017). Phylogenies were visualized in iTOL (Letunic and Bork, 2021) and annotated manually for taxonomy.

Additionally, we used AlphaFold3 website (Abramson et al., 2024) for identifying structurally similar proteins in the AlphaFold3 database (AFDB50). As query we used the protein sequences of *At*CLRP23 (Q8GXB1) and investigated the taxonomic distribution across hits with a pLDDT≥70 to represent strong overall structural similarity and backbone similarity. Taxonomic identification of hits was done by recovering the TaxID for the genus a particular hit corresponded to.

To investigate residue conservation, the BLASTp search function in Phytozome 13 (Goodstein et al., 2011) was used to identify CLRP23 homologs across a list of nine land plant species spanning dicots, monocots, lycophytes and bryophytes (references for the sequence databases are provided in Supplementary Methods S1). CLC Main Workbench 20.0.4 (QIAGEN, Aarhus, Denmark) was used to conduct sequence alignment with CLRP23 in Arabidopsis.

Statistical analysis and data availability

In addition to the software mentioned above, Microsoft Excel, GraphPad Prism, R and R studio were also used for statistical analysis and data visualisation. Raw data files of transcriptomic, proteomic and lipidomic analysis can be found on DataPlant (Schwenkert et. al. 2025, doi: 10.60534/qsh62-7p088, https://www.nfdi4plants.de/).

Supplementary data files

Supplementary Table S1: Envelope proteomics

Supplementary Table S2: Transcriptomics Cold Treatment

Supplementary Table S3: Proteomics Cold Treatment

Supplementary Table S4: Lipidomics Cold Treatment

Supplementary Table S5: Lipidomics Freezing Recovery

Supplementary Table S6: Sequence homology

Acknowledgements

CRISPR/Cas9 vectors were generously provided by Marc Youles (The Sainsbury Lab, Synthetic Biology), Silvestre Marillonnet (Leibniz Institute of Plant Biochemistry Halle, Synthetic Biology), and Cyril Zipfel (University of Zurich, Molecular and Cellular Plant Physiology). We sincerely thank Benjamin Brandt for his assistance with CRISPR/Cas9 construct design. We also express our gratitude to the MSBioLMU mass spectrometry service unit, particularly Yulia Davydova, for outstanding technical support. Additionally, we acknowledge Nadia Al-Thour and Tim Lücke for their valuable help with experiments. We also thank Timo Mühlhaus, David Zimmer and the DataPLANT consortium for supporting data archiving following the FAIR data principles (https://www.nfdi4plants.de/) and the Graduate School Life Science Munich (LSM) for their support. Artificial intelligence tools ChatGPT and Deepl were used to help write code and improve language. This research was funded by the German Research Foundation (DFG) TRR175, with support to SS (B06), DL (B07), HHK (B09), HEN (B03), and TK (C01).

Author contributions

SS designed the research and supervised the study. WTL, DW, MM, ML, TK, EA, BB, KS, KWE and DB performed research and analysed data. SS, CT, CG, HEN, SV, HHK and DL analysed data. WTL and SS wrote the paper with contributions of all authors.

References

Abramson, J., Adler, J., Dunger, J., Evans, R., Green, T., Pritzel, A., Ronneberger, O., Willmore, L., Ballard, A.J., Bambrick, J., Bodenstein, S.W., Evans, D.A., Hung, C.C., O'Neill, M., Reiman, D., Tunyasuvunakool, K., Wu, Z., Zemgulyte, A., Arvaniti, E., Beattie, C., Bertolli, O., Bridgland, A., Cherepanov, A., Congreve, M., Cowen-Rivers, A.I., Cowie, A., Figurnov, M., Fuchs, F.B., Gladman, H., Jain, R., Khan, Y.A., Low, C.M.R., Perlin, K., Potapenko, A., Savy, P., Singh, S., Stecula, A., Thillaisundaram, A., Tong, C., Yakneen, S., Zhong, E.D., Zielinski, M., Zidek, A., Bapst, V., Kohli, P., Jaderberg, M., Hassabis, D., and Jumper, J.M. (2024). Accurate structure prediction of biomolecular interactions with AlphaFold 3. Nature **630,** 493-500.

Awai, K., Maréchal, E., Block, M.A., Brun, D., Masuda, T., Shimada, H., Takamiya, K.-i., Ohta, H., and Joyard, J. (2001). Two types of MGDG synthase genes, found widely in both 16:3 and 18:3 plants, differentially mediate galactolipid syntheses in photosynthetic and nonphotosynthetic tissues in Arabidopsis thaliana. Proceedings of the National Academy of Sciences **98,** 10960-10965.

809 **Barkan, L., Vijayan, P., Carlsson, A.S., Mekhedov, S., and Browse, J.** (2006). A Suppressor of
810 fab1 Challenges Hypotheses on the Role of Thylakoid Unsaturation in Photosynthetic
811 Function. Plant Physiology **141,** 1012-1020.
812 **Barrero-Sicilia, C., Silvestre, S., Haslam, R.P., and Michaelson, L.V.** (2017). Lipid remodelling:
813 Unravelling the response to cold stress in Arabidopsis and its extremophile relative
814 Eutrema salsugineum. Plant Science **263,** 194-200.
815 **Block, M.A., Douce, R., Joyard, J., and Rolland, N.** (2007). Chloroplast envelope membranes:
816 a dynamic interface between plastids and the cytosol. Photosynthesis Research **92,**
817 225-244.
818 **Bobrovskikh, A.V., Zubairova, U.S., Bondar, E.I., Lavrekha, V.V., and Doroshkov, A.V.** (2022).
819 Transcriptomic Data Meta-Analysis Sheds Light on High Light Response in Arabidopsis
820 thaliana L. International Journal of Molecular Sciences **23,** 4455.
821 **Bölter, B., Mitterreiter, M., Schwenkert, S., Finkemeier, I., and Kunz, H.-H.** (2020). The
822 topology of plastid inner envelope potassium cation efflux antiporter KEA1 provides
823 new insights into its regulatory features. Photosynthesis Research **145**.
824 **Clough, S.J., and Bent, A.F.** (1998). Floral dip: a simplified method for Agrobacterium-
825 mediated transformation of Arabidopsis thaliana. The plant journal **16,** 735-743.
826 **Degenkolbe, T., Giavalisco, P., Zuther, E., Seiwert, B., Hincha, D.K., and Willmitzer, L.** (2012).
827 Differential remodeling of the lipidome during cold acclimation in natural accessions
828 of Arabidopsis thaliana. The Plant Journal **72,** 972-982.
829 **Di Ferdinando, M., Brunetti, C., Fini, A., and Tattini, M.** (2012). Flavonoids as antioxidants in
830 plants under abiotic stresses. Abiotic stress responses in plants: metabolism,
831 productivity and sustainability**,** 159-179.
832 **Dischinger, A., and Schwenkert, S.** (2022). Chloroplast Envelope Membrane Subfractionation
833 from Arabidopsis and Pea. In Plant Proteostasis: Methods and Protocols (Springer), pp.
834 267-284.
835 **Dörmann, P., Balbo, I., and Benning, C.** (1999). Arabidopsis galactolipid biosynthesis and lipid
836 trafficking mediated by DGD1. Science **284,** 2181-2184.
837 **Dyall, S.D., Brown, M.T., and Johnson, P.J.** (2004). Ancient Invasions: From Endosymbionts to
838 Organelles. Science **304,** 253-257.
839 **Eberhardt, J., Santos-Martins, D., Tillack, A.F., and Forli, S.** (2021). AutoDock Vina 1.2.0: New
840 Docking Methods, Expanded Force Field, and Python Bindings. Journal of Chemical
841 Information and Modeling **61,** 3891-3898.
842 **Eisa, A., Malenica, K., Schwenkert, S., and Bölter, B.** (2020). High Light Acclimation Induces
843 Chloroplast Precursor Phosphorylation and Reduces Import Efficiency. Plants **9,** 24.
844 **Eme, L., Tamarit, D., Caceres, E.F., Stairs, C.W., De Anda, V., Schon, M.E., Seitz, K.W.,**
845 **Dombrowski, N., Lewis, W.H., Homa, F., Saw, J.H., Lombard, J., Nunoura, T., Li, W.J.,**
846 **Hua, Z.S., Chen, L.X., Banfield, J.F., John, E.S., Reysenbach, A.L., Stott, M.B., Schramm,**
847 **A., Kjeldsen, K.U., Teske, A.P., Baker, B.J., and Ettema, T.J.G.** (2023). Inference and
848 reconstruction of the heimdallarchaeial ancestry of eukaryotes. Nature **618,** 992-999.
849 **Fan, J., Zhai, Z., Yan, C., and Xu, C.** (2015). Arabidopsis TRIGALACTOSYLDIACYLGLYCEROL5
850 interacts with TGD1, TGD2, and TGD4 to facilitate lipid transfer from the endoplasmic
851 reticulum to plastids. The Plant Cell **27,** 2941-2955.
852 **Froehlich, J.** (2011). Studying Arabidopsis Envelope Protein Localization and Topology Using
853 Thermolysin and Trypsin Proteases. In Chloroplast Research in Arabidopsis: Methods
854 and Protocols, Volume I, R.P. Jarvis, ed (Totowa, NJ: Humana Press), pp. 351-367.
855 **Goetze, T.A., Patil, M., Jeshen, I., Bölter, B., Grahl, S., and Soll, J.** (2015). Oep23 forms an ion
856 channel in the chloroplast outer envelope. BMC Plant Biology **15,** 47.

857 **Goodstein, D.M., Shu, S., Howson, R., Neupane, R., Hayes, R.D., Fazo, J., Mitros, T., Dirks,**
858 **W., Hellsten, U., Putnam, N., and Rokhsar, D.S.** (2011). Phytozome: a comparative
859 platform for green plant genomics. Nucleic Acids Research **40,** D1178-D1186.
860 **Gould, S.B., Garg, S.G., and Martin, W.F.** (2016). Bacterial Vesicle Secretion and the
861 Evolutionary Origin of the Eukaryotic Endomembrane System. Trends Microbiol **24,**
862 525-534.
863 **Gounaris, K., Mannock, D., Sen, A., Brain, A., Williams, W., and Quinn, P.** (1983).
864 Polyunsaturated fatty acyl residues of galactolipids are involved in the control of
865 bilayer/non-bilayer lipid transitions in higher plant chloroplasts. Biochimica et
866 Biophysica Acta (BBA)-Biomembranes **732,** 229-242.
867 **Gruner, S.M., Cullis, P.R., Hope, M.J., and Tilcock, C.P.** (1985). Lipid polymorphism: the
868 molecular basis of nonbilayer phases. Annu Rev Biophys Biophys Chem **14,** 211-238.
869 **Grützner, R., Martin, P., Horn, C., Mortensen, S., Cram, E.J., Lee-Parsons, C.W.T., Stuttmann,**
870 **J., and Marillonnet, S.** (2021). High-efficiency genome editing in plants mediated by a
871 Cas9 gene containing multiple introns. Plant Communications **2**.
872 **Hannah, M.A., Heyer, A.G., and Hincha, D.K.** (2005). A Global Survey of Gene Regulation
873 during Cold Acclimation in Arabidopsis thaliana. PLOS Genetics **1,** e26.
874 **Hölzl, G., and Dörmann, P.** (2019). Chloroplast Lipids and Their Biosynthesis. Annual Review
875 of Plant Biology **70,** 51-81.
876 **Hölzl, G., and Dörmann, P.** (2021). Thin-Layer Chromatography, pp. 29-41.
877 **Huang, D.W., Sherman, B.T., and Lempicki, R.A.** (2009). Systematic and integrative analysis
878 of large gene lists using DAVID bioinformatics resources. Nat Protoc **4,** 44-57.
879 **Hugly, S., and Somerville, C.** (1992). A Role for Membrane Lipid Polyunsaturation in
880 Chloroplast Biogenesis at Low Temperature 1. Plant Physiology **99,** 197-202.
881 **Hummel, J., Segu, S., Li, Y., Irgang, S., Jueppner, J., and Giavalisco, P.** (2011). Ultra
882 Performance Liquid Chromatography and High Resolution Mass Spectrometry for the
883 Analysis of Plant Lipids. Frontiers in Plant Science **2**.
884 **Jalili, V., Afgan, E., Gu, Q., Clements, D., Blankenberg, D., Goecks, J., Taylor, J., and**
885 **Nekrutenko, A.** (2020). The Galaxy platform for accessible, reproducible and
886 collaborative biomedical analyses: 2020 update. Nucleic acids research **48,** W395-
887 W402.
888 **John, A., Keller, I., Ebel, K.W., and Neuhaus, H.E.** (2024). Two critical membranes: how does
889 the chloroplast envelope affect plant acclimation properties? Journal of Experimental
890 Botany **76,** 214-227.
891 **Jumper, J., Evans, R., Pritzel, A., Green, T., Figurnov, M., Ronneberger, O., Tunyasuvunakool,**
892 **K., Bates, R., Žídek, A., Potapenko, A., Bridgland, A., Meyer, C., Kohl, S.A.A., Ballard,**
893 **A.J., Cowie, A., Romera-Paredes, B., Nikolov, S., Jain, R., Adler, J., Back, T., Petersen,**
894 **S., Reiman, D., Clancy, E., Zielinski, M., Steinegger, M., Pacholska, M., Berghammer,**
895 **T., Bodenstein, S., Silver, D., Vinyals, O., Senior, A.W., Kavukcuoglu, K., Kohli, P., and**
896 **Hassabis, D.** (2021). Highly accurate protein structure prediction with AlphaFold.
897 Nature **596,** 583-589.
898 **Kalyaanamoorthy, S., Minh, B.Q., Wong, T.K.F., von Haeseler, A., and Jermiin, L.S.** (2017).
899 ModelFinder: fast model selection for accurate phylogenetic estimates. Nat Methods
900 **14,** 587-589.
901 **Karimi, M., Inzé, D., and Depicker, A.** (2002). GATEWAY™ vectors for Agrobacterium-
902 mediated plant transformation. Trends in plant science **7,** 193-195.
903 **Katoh, K., and Standley, D.M.** (2013). MAFFT multiple sequence alignment software version
904 7: improvements in performance and usability. Mol Biol Evol **30,** 772-780.

905 **Kelly, A.A., and Dörmann, P.** (2002). DGD2, an Arabidopsis Gene Encoding a UDP-Galactose-
906 dependent Digalactosyldiacylglycerol Synthase Is Expressed during Growth under
907 Phosphate-limiting Conditions *. Journal of Biological Chemistry **277,** 1166-1173.
908 **Kim, J., Na, Y.J., Park, S.J., Baek, S.-H., and Kim, D.H.** (2019). Biogenesis of chloroplast outer
909 envelope membrane proteins. Plant Cell Reports **38,** 783-792.
910 **Kim, S., Chen, J., Cheng, T., Gindulyte, A., He, J., He, S., Li, Q., Shoemaker, Benjamin A.,**
911 **Thiessen, Paul A., Yu, B., Zaslavsky, L., Zhang, J., and Bolton, Evan E.** (2025). PubChem
912 2025 update. Nucleic Acids Research **53,** D1516-D1525.
913 **Kitashova, A., Lehmann, M., Schwenkert, S., Münch, M., Leister, D., and Nägele, T.** (2024).
914 Insights into physiological roles of flavonoids in plant cold acclimation. The Plant
915 Journal **120,** 2269-2285.
916 **Kitashova, A., Adler, S.O., Richter, A.S., Eberlein, S., Dziubek, D., Klipp, E., and Nägele, T.**
917 (2023). Limitation of sucrose biosynthesis shapes carbon partitioning during plant cold
918 acclimation. Plant, cell & environment **46,** 464-478.
919 **Kleine, T., Nägele, T., Neuhaus, H.E., Schmitz-Linneweber, C., Fernie, A.R., Geigenberger, P.,**
920 **Grimm, B., Kaufmann, K., Klipp, E., Meurer, J., Möhlmann, T., Mühlhaus, T., Naranjo,**
921 **B., Nickelsen, J., Richter, A., Ruwe, H., Schroda, M., Schwenkert, S., Trentmann, O.,**
922 **Willmund, F., Zoschke, R., and Leister, D.** (2021). Acclimation in plants – the Green
923 Hub consortium. The Plant Journal **106,** 23-40.
924 **Klughammer, C., and Schreiber, U.** (2008). Complementary PS II quantum yields calculated
925 from simple fluorescence parameters measured by PAM fluorometry and the
926 Saturation Pulse method. PAM application notes **1,** 201-247.
927 **Laemmli, U.K.** (1970). Cleavage of Structural Proteins during the Assembly of the Head of
928 Bacteriophage T4. Nature **227,** 680-685.
929 **Leister, D., and Kleine, T.** (2008). Towards a comprehensive catalog of chloroplast proteins
930 and their interactions. Cell Research **18,** 1081-1083.
931 **Leonova, S., Shelenga, T., Hamberg, M., Konarev, A.V., Loskutov, I., and Carlsson, A.S.** (2008).
932 Analysis of Oil Composition in Cultivars and Wild Species of Oat (Avena sp.). Journal of
933 Agricultural and Food Chemistry **56,** 7983-7991.
934 **Letunic, I., and Bork, P.** (2021). Interactive Tree Of Life (iTOL) v5: an online tool for
935 phylogenetic tree display and annotation. Nucleic Acids Res **49,** W293-W296.
936 **Li, J., Liu, L.-N., Meng, Q., Fan, H., and Sui, N.** (2020). The roles of chloroplast membrane lipids
937 in abiotic stress responses. Plant Signaling & Behavior **15,** 1807152.
938 **Li, N., Gügel, I.L., Giavalisco, P., Zeisler, V., Schreiber, L., Soll, J., and Philippar, K.** (2015).
939 FAX1, a Novel Membrane Protein Mediating Plastid Fatty Acid Export. PLOS Biology **13,**
940 e1002053.
941 **Love, M.I., Huber, W., and Anders, S.** (2014). Moderated estimation of fold change and
942 dispersion for RNA-seq data with DESeq2. Genome biology **15,** 1-21.
943 **MacDonald, M.T., Lada, R.R., MacDonald, G.E., Caldwell, C.D., and Udenigwe, C.C.** (2023).
944 Changes in Polar Lipid Composition in Balsam Fir during Seasonal Cold Acclimation and
945 Relationship to Needle Abscission. International Journal of Molecular Sciences **24,**
946 15702.
947 **Martin, W., Stoebe, B., Goremykin, V., Hansmann, S., Hasegawa, M., and Kowallik, K.V.**
948 (1998). Gene transfer to the nucleus and the evolution of chloroplasts. Nature **393,**
949 162-165.
950 **Miura, K., and Furumoto, T.** (2013). Cold signaling and cold response in plants. Int J Mol Sci
951 **14,** 5312-5337.

Moellering, E.R., Muthan, B., and Benning, C. (2010). Freezing tolerance in plants requires lipid remodeling at the outer chloroplast membrane. Science **330,** 226-228.

Morris, G.M., Huey, R., Lindstrom, W., Sanner, M.F., Belew, R.K., Goodsell, D.S., and Olson, A.J. (2009). AutoDock4 and AutoDockTools4: Automated docking with selective receptor flexibility. Journal of Computational Chemistry **30,** 2785-2791.

Murakami, Y., Tsuyama, M., Kobayashi, Y., Kodama, H., and Iba, K. (2000). Trienoic Fatty Acids and Plant Tolerance of High Temperature. Science **287,** 476-479.

Nguyen, L.T., Schmidt, H.A., von Haeseler, A., and Minh, B.Q. (2015). IQ-TREE: a fast and effective stochastic algorithm for estimating maximum-likelihood phylogenies. Mol Biol Evol **32,** 268-274.

O'Boyle, N.M., Banck, M., James, C.A., Morley, C., Vandermeersch, T., and Hutchison, G.R. (2011). Open Babel: An open chemical toolbox. Journal of Cheminformatics **3,** 33.

Pålsson, D., Penttinen, H., Malmberg, C., Adlercreutz, P., and Tullberg, C. (2024). Rancidity development in oat during industrial processing. LWT **204,** 116448.

Petrussa, E., Braidot, E., Zancani, M., Peresson, C., Bertolini, A., Patui, S., and Vianello, A. (2013). Plant Flavonoids—Biosynthesis, Transport and Involvement in Stress Responses. International Journal of Molecular Sciences **14,** 14950-14973.

Pettersen, E.F., Goddard, T.D., Huang, C.C., Couch, G.S., Greenblatt, D.M., Meng, E.C., and Ferrin, T.E. (2004). UCSF Chimera—A visualization system for exploratory research and analysis. Journal of Computational Chemistry **25,** 1605-1612.

Radauer, C., Lackner, P., and Breiteneder, H. (2008). The Bet v 1 fold: an ancient, versatile scaffold for binding of large, hydrophobic ligands. BMC Evolutionary Biology **8,** 286.

Rappsilber, J., Ishihama, Y., and Mann, M. (2003). Stop and go extraction tips for matrix-assisted laser desorption/ionization, nanoelectrospray, and LC/MS sample pretreatment in proteomics. Analytical chemistry **75,** 663-670.

Routaboul, J.-M., Fischer, S.F., and Browse, J. (2000). Trienoic Fatty Acids Are Required to Maintain Chloroplast Function at Low Temperatures1. Plant Physiology **124,** 1697-1705.

Scherer, V., Bellin, L., Schwenkert, S., Lehmann, M., Rinne, J., Witte, C.-P., Jahnke, K., Richter, A., Pruss, T., Lau, A., Waller, L., Stein, S., Leister, D., and Möhlmann, T. (2024). Uracil phosphoribosyltransferase is required to establish a functional cytochrome b6f complex. The Plant Journal **120,** 1064-1078.

Schrodinger, L. (2010). The PyMOL Molecular Graphics System. Version 3.1.1.

Schwenkert, S., Leister, D., and Lo, W.T. (2023a). Hidden keyholders – exploring metabolite transport across the outer chloroplast membrane. Journal of Mitochondria, Plastids and Endosymbiosis **1,** 2247168.

Schwenkert, S., Fernie, A.R., Geigenberger, P., Leister, D., Möhlmann, T., Naranjo, B., and Neuhaus, H.E. (2022). Chloroplasts are key players to cope with light and temperature stress. Trends in Plant Science **27,** 577-587.

Schwenkert, S., Lo, W.T., Szulc, B., Yip, C.K., Pratt, A.I., Cusack, S.A., Brandt, B., Leister, D., and Kunz, H.-H. (2023b). Probing the physiological role of the plastid outer-envelope membrane using the oemiR plasmid collection. G3: Genes, Genomes, Genetics **13,** jkad187.

Seiwert, D., Witt, H., Janshoff, A., and Paulsen, H. (2017). The non-bilayer lipid MGDG stabilizes the major light-harvesting complex (LHCII) against unfolding. Scientific Reports **7,** 5158.

Sherman, B.T., Hao, M., Qiu, J., Jiao, X., Baseler, M.W., Lane, H.C., Imamichi, T., and Chang, W. (2022). DAVID: a web server for functional enrichment analysis and functional annotation of gene lists (2021 update). Nucleic Acids Res **50,** W216-w221.

Shimada, T.L., Shimada, T., and Hara-Nishimura, I. (2010). A rapid and non-destructive screenable marker, FAST, for identifying transformed seeds of Arabidopsis thaliana. The Plant Journal **61,** 519-528.

Shimojima, M., Ohta, H., Iwamatsu, A., Masuda, T., Shioi, Y., and Takamiya, K.-i. (1997). Cloning of the gene for monogalactosyldiacylglycerol synthase and its evolutionary origin. Proceedings of the National Academy of Sciences **94,** 333-337.

Shomali, A., Das, S., Arif, N., Sarraf, M., Zahra, N., Yadav, V., Aliniaeifard, S., Chauhan, D.K., and Hasanuzzaman, M. (2022). Diverse physiological roles of flavonoids in plant environmental stress responses and tolerance. Plants **11,** 3158.

Singh, U.C., and Kollman, P.A. (1984). An approach to computing electrostatic charges for molecules. Journal of Computational Chemistry **5,** 129-145.

Soccio, R.E., and Breslow, J.L. (2003). StAR-related lipid transfer (START) proteins: mediators of intracellular lipid metabolism. Journal of Biological Chemistry **278,** 22183-22186.

Soll, J., and Schleiff, E. (2004). Protein import into chloroplasts. Nature Reviews Molecular Cell Biology **5,** 198-208.

Tang, Q., Xu, D., Lenzen, B., Brachmann, A., Yapa, M.M., Doroodian, P., Schmitz-Linneweber, C., Masuda, T., Hua, Z., and Leister, D. (2024). GENOMES UNCOUPLED PROTEIN1 binds to plastid RNAs and promotes their maturation. Plant Communications **5**.

Trentmann, O., Mühlhaus, T., Zimmer, D., Sommer, F., Schroda, M., Haferkamp, I., Keller, I., Pommerrenig, B., and Neuhaus, H.E. (2020). Identification of Chloroplast Envelope Proteins with Critical Importance for Cold Acclimation1 [OPEN]. Plant Physiology **182,** 1239-1255.

Trott, O., and Olson, A.J. (2010). AutoDock Vina: Improving the speed and accuracy of docking with a new scoring function, efficient optimization, and multithreading. Journal of Computational Chemistry **31,** 455-461.

Ursache, R., Fujita, S., Dénervaud Tendon, V., and Geldner, N. (2021). Combined fluorescent seed selection and multiplex CRISPR/Cas9 assembly for fast generation of multiple Arabidopsis mutants. Plant Methods **17,** 1-14.

Varadi, M., Bertoni, D., Magana, P., Paramval, U., Pidruchna, I., Radhakrishnan, M., Tsenkov, M., Nair, S., Mirdita, M., Yeo, J., Kovalevskiy, O., Tunyasuvunakool, K., Laydon, A., Žídek, A., Tomlinson, H., Hariharan, D., Abrahamson, J., Green, T., Jumper, J., Birney, E., Steinegger, M., Hassabis, D., and Velankar, S. (2023). AlphaFold Protein Structure Database in 2024: providing structure coverage for over 214 million protein sequences. Nucleic Acids Research **52,** D368-D375.

Varadi, M., Anyango, S., Deshpande, M., Nair, S., Natassia, C., Yordanova, G., Yuan, D., Stroe, O., Wood, G., Laydon, A., Žídek, A., Green, T., Tunyasuvunakool, K., Petersen, S., Jumper, J., Clancy, E., Green, R., Vora, A., Lutfi, M., Figurnov, M., Cowie, A., Hobbs, N., Kohli, P., Kleywegt, G., Birney, E., Hassabis, D., and Velankar, S. (2022). AlphaFold Protein Structure Database: massively expanding the structural coverage of protein-sequence space with high-accuracy models. Nucleic Acids Research **50,** D439-D444.

Vicente, A.M., Manavski, N., Rohn, P.T., Schmid, L.-M., Garcia-Molina, A., Leister, D., Seydel, C., Bellin, L., Möhlmann, T., Ammann, G., Kaiser, S., and Meurer, J. (2023). The plant cytosolic m⁶A RNA methylome stabilizes photosynthesis in the cold. Plant Communications **4**.

1045 **Vojta, L., Soll, J., and Bölter, B.** (2007). Protein transport in chloroplasts− targeting to the
1046 intermembrane space. The FEBS journal **274,** 5043-5054.
1047 **Waegemann, K., Eichacker, S., and Soll, J.** (1992). Outer envelope membranes from
1048 chloroplasts are isolated as right-side-out vesicles. Planta **187,** 89-94.
1049 **Webb, M.S., and Green, B.R.** (1991). Biochemical and biophysical properties of thylakoid acyl
1050 lipids. Biochimica et Biophysica Acta (BBA)-Bioenergetics **1060,** 133-158.
1051 **Weber, A.P., Schwacke, R., and Flügge, U.-I.** (2005). Solute transporters of the plastid
1052 envelope membrane. Annu. Rev. Plant Bio. **56,** 133-164.
1053 **Weber, A.P.M., and Fischer, K.** (2009). The Role of Metabolite Transporters in Integrating
1054 Chloroplasts with the Metabolic Network of Plant Cells. In The Chloroplast:
1055 Interactions with the Environment, A.S. Sandelius and H. Aronsson, eds (Berlin,
1056 Heidelberg: Springer Berlin Heidelberg), pp. 159-179.
1057 **Wiśniewski, J.R., Zougman, A., Nagaraj, N., and Mann, M.** (2009). Universal sample
1058 preparation method for proteome analysis. Nature methods **6,** 359-362.
1059 **Yoshihara, A., and Kobayashi, K.** (2022). Lipids in photosynthetic protein complexes in the
1060 thylakoid membrane of plants, algae, and cyanobacteria. Journal of Experimental
1061 Botany **73,** 2735-2750.
1062 **Yu, C.W., Lin, Y.T., and Li, H.m.** (2020). Increased ratio of galactolipid MGDG: DGDG induces
1063 jasmonic acid overproduction and changes chloroplast shape. New Phytologist **228,**
1064 1327-1335.
1065 **Zheng, G., Li, L., and Li, W.** (2016). Glycerolipidome responses to freezing- and chilling-induced
1066 injuries: examples in Arabidopsis and rice. BMC Plant Biology **16,** 70.

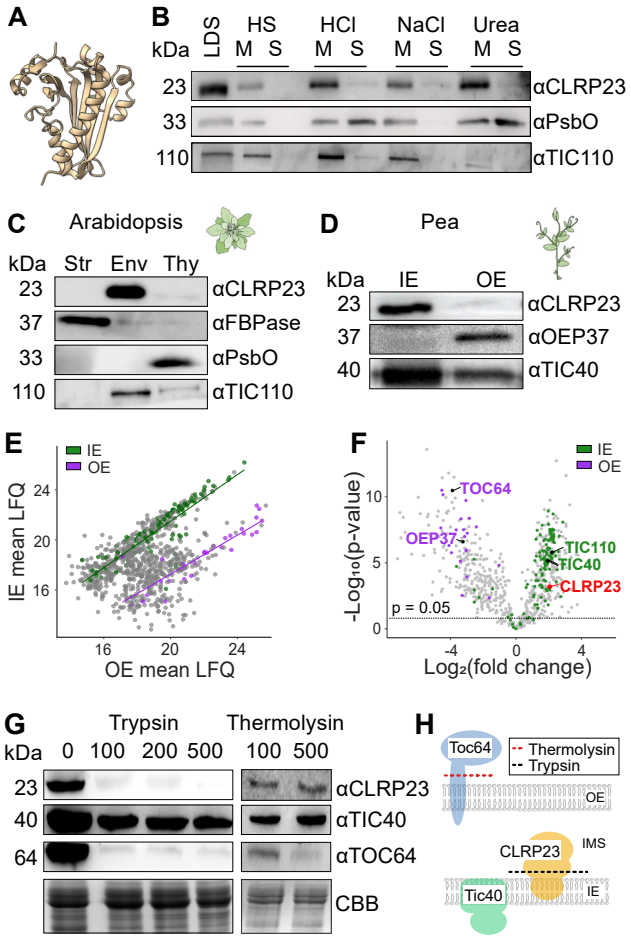

Figure 1: Localization of CLRP23 to the IE and IMS. A) CLRP23 structure prediction found in AlphaFold DB. **B)** Membrane association of CLRP23. Arabidopsis leaves (approx. 500 mg FW) were ground with liquid nitrogen and treated with LDS, buffer (HS), HCl, NaCl or Urea and subsequently separated into soluble (S) and membrane (M) fractions. Samples were separated on SDS gels, transferred onto PVDF and immunolabeled with α-CLRP23, α-PsbO, and α-Tic110. **C)** Arabidopsis chloroplasts were fractionated into Str, Env and Thy. **D)** Pea chloroplasts were fractionated into IE and OE. Samples were separated on SDS gels, transferred onto PVDF membranes and immunolabeled with αCLRP23, αFBPase, αPsbO, αTIC110 in (C) and αCLRP23, αOEP37, and αTIC40 in (D). **E)** Scatter plot comparing the mean LFQ intensities of proteins identified in IE and OE fractions of pea chloroplasts measured by mass spectrometry. Each point represents an individual protein, with IE proteins shown in green and OE proteins in purple. Trend lines were fitted separately for the two fractions. **F)** Volcano plot showing differentially abundant proteins in the chloroplast IE vs OE fractions based on mass spectrometric analysis. The $\log_2$ fold change is plotted against the negative $\log_{10}$ of the adjusted p-value. Differentially abundant proteins were identified by a Student's *t*-test (permutation-based FDR = 0.05). Proteins known to reside in the IE and OE are highlighted in green and purple, respectively. CLRP23 is labeled in red. **G)** Protease treatment of Arabidopsis chloroplasts. Intact chloroplasts of WT were treated with 0, 100, 200, 500 or 1000 µg Trypsin or 100 or 500 µg Thermolysin/mg chlorophyll. Samples corresponding to 15 µg chlorophyll were separated on SDS gels, transferred onto PVDF and immunolabeled with α-CLRP23, α-Tic40, and α-Toc64, respectively. Molecular sizes are indicated on the left and CBB is shown as a loading control. **H)** Schematic showing CLBP topology as determined in (G). The protease treatment and expected cleavages of Toc64 and CLRP23 is shown as dotted lines. CLRP23 is concluded to face the IMS.

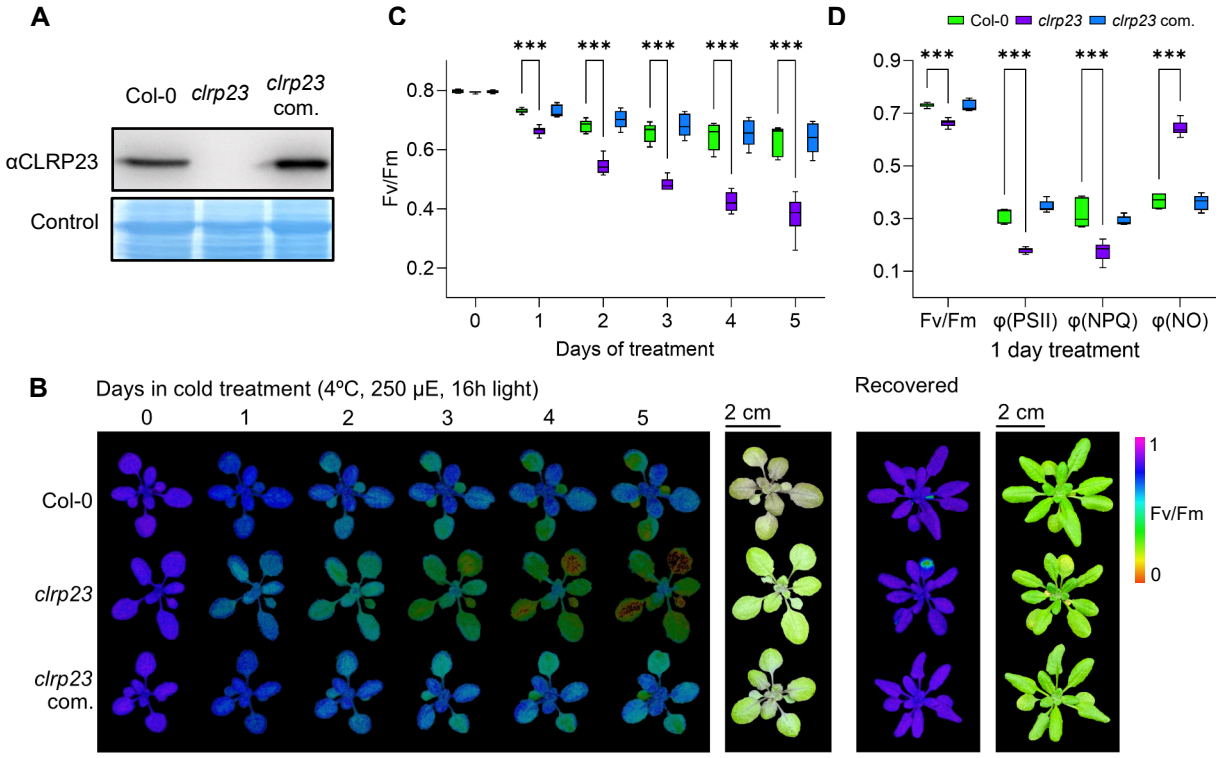

Figure 2: Cold sensitive phenotype of *clrp23* mutants under cold and high light conditions. Col-0, *clrp23* and complemented plants were grown under standard growth conditions for 21 days before transferring to cold and high light conditions (4ºC, 250 µE, 16h light). After 6 days of treatment, plants were transferred back to standard growth conditions for 1 week to recover. Chl α fluorescence measurements were taken from 0 to 5 days of treatment and 1 week after recovery. **A)** Total protein extracts from Col-0, *clrp23* and complemented plants (clrp23 com) were separated with SDS-PAGE, transferred onto a PVDF membrane and immunolabeled with αCLRP23 at 23 kDa, with CBB shown as a loading control. **B)** Chlorophyll fluorescence imaging during cold and high light treatment and after 1 week of recovery. **C)** Fv/Fm values after 0-5 days of cold and high light treatment. **D)** Fv/Fm, PSII quantum yield (φ(PSII)), non-photochemical quenching (φ(NPQ)) and nonregulated energy dissipation (φ(NO)) after 1 day of cold and high light treatment. Asterisks indicate statistically significant differences according to Student's *t*-test (*p<0.05; **p<0.01; ***p<0.001).

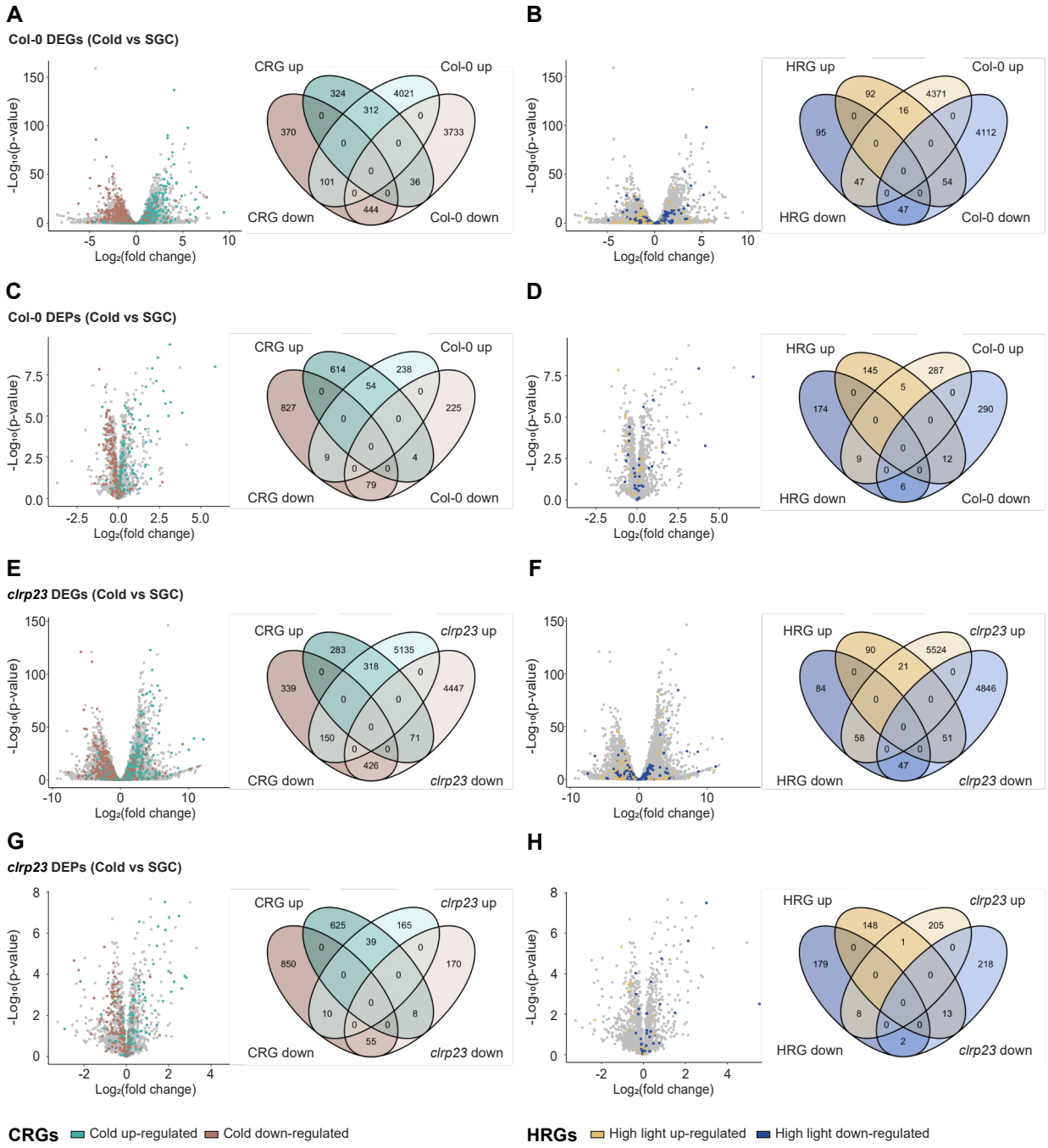

Figure 3: DEGs (A, B, E, F) and DEPs (C, D, G, H) in Col-0 (A-D) and *clrp23* (E-H) after cold treatment vs SGC, in the context of published meta-analyses. Each dot represents one gene/protein, plotted according to $-\log_{10}$ adjusted p-value and $\log_2$ fold change. DEGs were identified with DESeq2. DEPs were identified by a Student's *t*-test (permutation-based FDR = 0.05). Genes and proteins found in published literature to be up and downregulated by >48 hours cold treatment (CRGs; Hannah et al., 2005) are highlighted in green and brown (A, C, E, G), while genes and proteins found in published literature to be up and downregulated by 48-120 hours high light treatment (HRGs; Bobrovskikh et al., 2022) are highlighted in yellow and blue (B, D, F, H), respectively. DEGs, differentially expressed genes; DEPs, differentially expressed proteins; SGC, standard growth conditions.

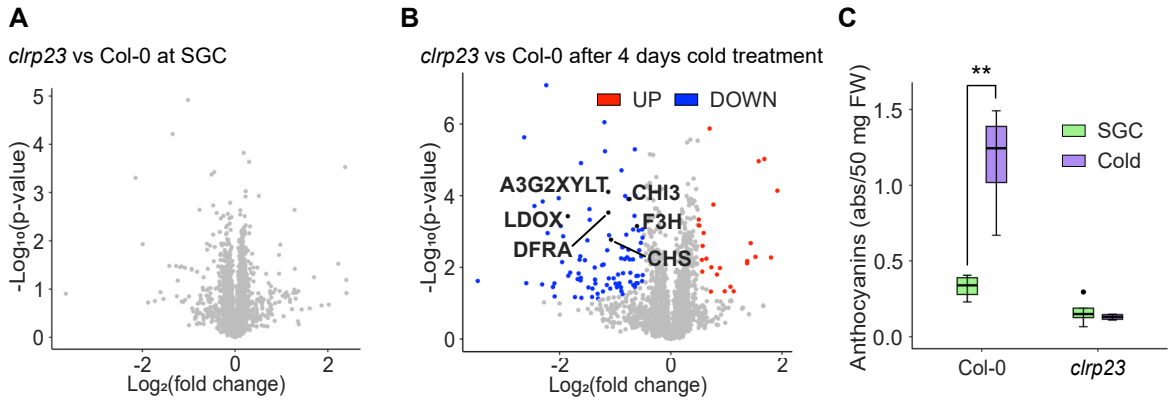

Figure 4: DEPs in *clrp23* vs Col-0 A) under SGC and B) after 4 days of cold treatment. GO biological process enrichment analysis of DEPs in *clrp23* under cold showed a downregulation in proteins involved in flavonoid biosynthesis, the proteins of which are labeled in the volcano plot. Each dot represents one protein, plotted according to $-\log_{10}$ adjusted p-value and $\log_2$ fold change. **C)** Reduced anthocyanin accumulation in *clrp23* mutants after cold treatment. Asterisks indicate statistically significant differences according to a Student's t-test (*p<0.05; **p<0.01; ***p<0.001). DEPs, differentially expressed proteins; SGC, standard growth conditions.

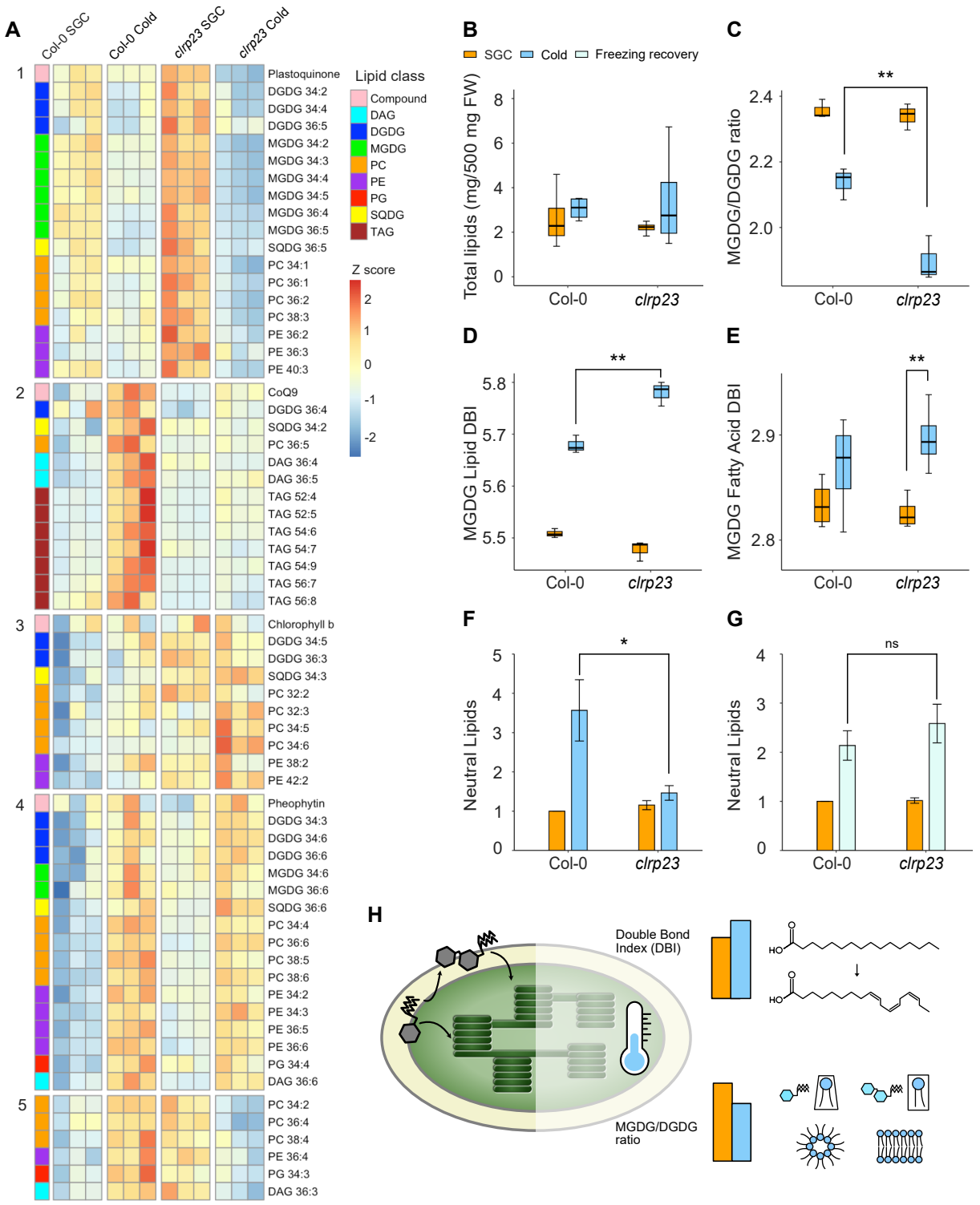

Figure 5: Lipid analysis of Col-0 and *clrp23* after cold treatment (4ºC, 250µE, 16h light). A) Heat map showing the z scores of all lipid species detected and quantified with LC-MS. Using k-means clustering, each lipid species is grouped into 1 of 5 clusters. **B)** Total lipids extracted and quantified with GC-FID in *clrp23* after cold treatment. **C)** MGDG/DGDG ratio in *clrp23* after cold treatment. MGDG/DGDG ratio was calculated from LC-MS data based on relative abundance (peak area in relation to the internal standard corticosterone). **(D-E)** Double bond index (DBI) of MGDG (D) lipid species and (E) fatty acids in *clrp23* after cold treatment. DBI was calculated by Σ % lipid or fatty acid*the number of double bonds in each lipid or fatty acid. DBI of MGDG lipids in (D) was calculated from LC-MS data based on relative abundance while DBI of MGDG fatty acids in (E) was calculated from GC-FID data based on mol%. **(F-G)** Neutral lipids quantified with LC-MS in *clrp23* mutants after (F) cold treatment (G) and freezing recovery, reported as abundance relative to Col-0 levels at standard growth conditions. Asterisks indicate statistically significant differences according to a Student's t-test (*p<0.05; **p<0.01; ***p<0.001). **H)** Schematic showing galactolipid synthesis at the chloroplast envelope and galactolipid remodeling under low temperature stress.

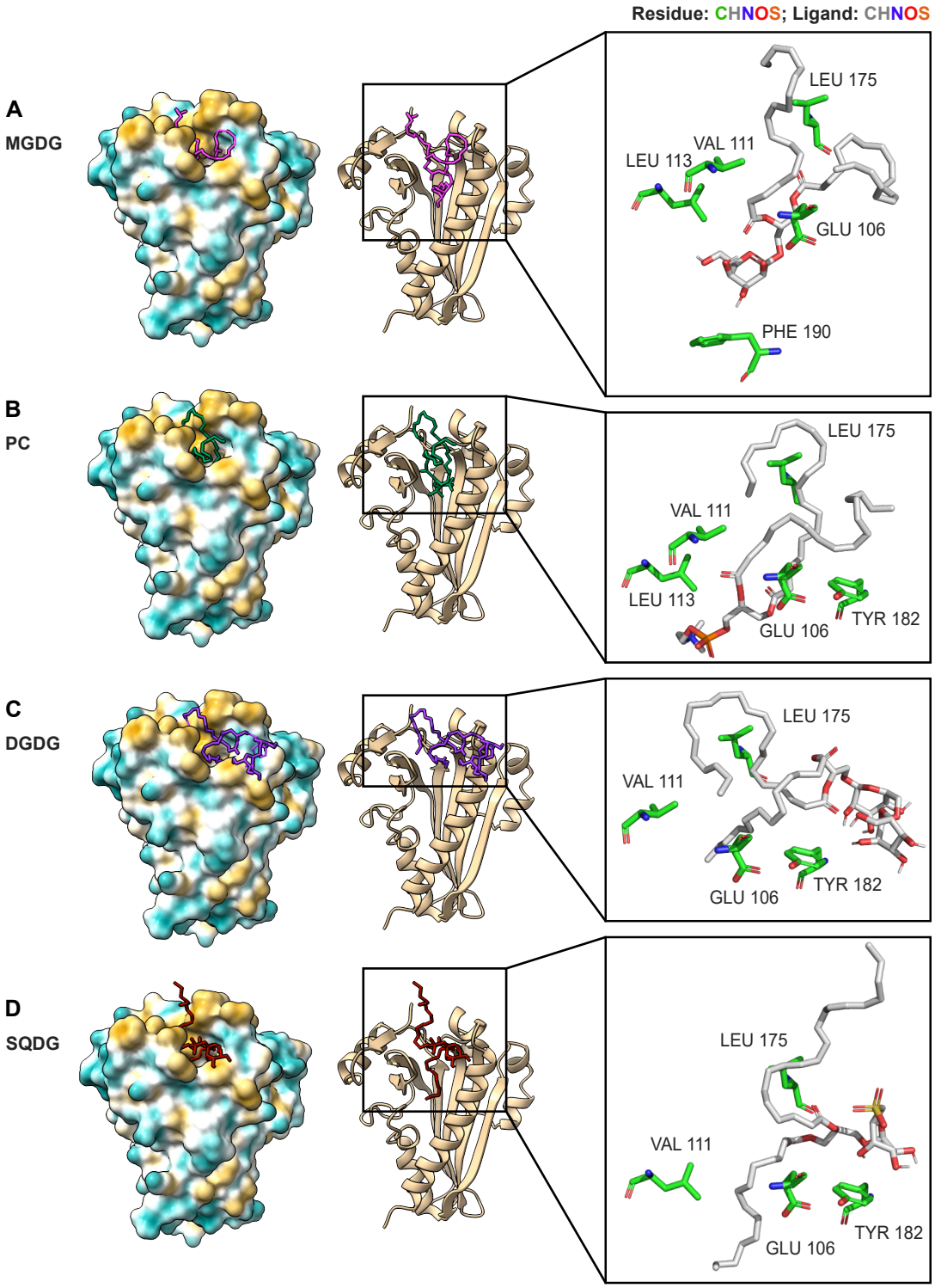

Figure 6: Molecular docking simulation of CLRP23 against A) MGDG, B) PC, C) DGDG and D) SQDG. CLRP23 is depicted using a ribbon diagram and a surface hydrophobicity map, colored from blue (hydrophilic) to yellow (hydrophobic). Ligand contact sites were identified using PyMol, highlighting residues common to at least three ligands. The F109 residue is also highlighted. Autodock 4.2 was used for molecular docking. ChimeraX-1.8 and PyMOL was used for visualization and identification of contact sites.

Residue	Distance (Å)				Dicots					Monocots		Lycophytes	Bryophytes
	MGDG	PC	DGDG	SQDG	*G. max*	*S. lycopersicum*	*P. trichocarpa*	*V. vinifera*	*A. trichopoda*	*O. sativa*	*Z. mays*	*S. moellendorffi*	*P. patens*
V2	3.3	-	3.2	-	L	V	V	V	-	-	L	-	L
I102	-	3.4	-	-	V	V	V	V	V	I	I	V	V
V104	3.4	-	-	3.4	V	V	V	T	T	Y	Y	S	A
E106	3.3	3.5	3.5	3.3	E	E	E	T	E	E	E	E	E
V107	-	-	-	3.4	F	F	F	F	F	L	L	G	L
L108	-	-	-	3.4	F	F	L	L	L	I	I	L	V
V111	3.4	3.4	3.5	-	L	L	V	T	V	V	V	I	I
L113	3.4	3.2	-	3.2	M	M	M	M	L	L	L	N	N
H143	3.4	3.2	-	-	H	H	H	H	H	H	H	H	H
E148	-	3.5	-	-	E	E	E	E	E	E	E	E	E
L175	3.5	3.4	3.5	3.2	L	L	L	L	L	L	L	L	L
S176	-	-	-	3.4	S	S	S	S	S	S	A	S	S
L178	-	-	3.2	-	V	F	I	L	M	L	L	A	A
Y182	-	3.4	2.9	3.2	Y	Y	Y	Y	Y	Y	Y	Y	V
V183	-	3.4	-	-	V	V	V	V	V	V	V	V	A
R186	3.3	3.3	-	-	R	R	R	M	R	R	R	K	Q
F190	2.5	-	-	-	F	F	F	F	F	F	F	F	F

Distance (Å)

< 3 | 3 < 3.5

Residue

Identical | Similar

Figure 7: Sequence alignment analysis of homologs of CLRP23 in Dicots, Monocots, Lycophytes and Bryophytes. Homologs of CLRP23 were identified in G. max (Glyma.16G120900.1.p), S. lycopersicum (Solyc02g083180.2.1), P. trichocarpa (Potri.005G105500.2), V. vinifera (VIT_200s0338g00020.1), A. trichopoda (evm_27.model.AmTr_v1.0_scaffold00001.98), O. sativa (LOC_Os03g01730.3), Z. mays (Zm00001d016543_P003), S. moellendorffi (36490), and P. patens (Pp3c1_37080V3.2.p). Residues identified as contact sites for MGDG, PC, DGDG and SQDG are shown as well as their respective distances to the ligand (Å). Residues in each homolog that are identical to that of At-CLRP23 are highlighted in bright green, while residues that are changed to an amino acid in the same category (hydrophobic, hydrophilic, acidic, or basic) are highlighted in a lighter green.

A

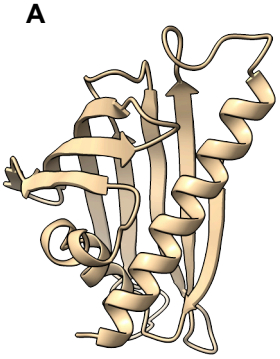

B

Rank	Template ID	Coverage (%)	Confidence	Sequence identity (%)
1	c2d4rA	73	86.4	12
2	c2d4rD	73	86.4	12
3	c2pcsA	72	82.1	8

Supplemental Figure S1: Structural prediction of CLRP23 with Phyre2.2 A) Visualisation of predicted structure of CLRP23 with UCSF ChimeraX-1.8. **B)** Topped ranked template IDs from structural prediction.

A

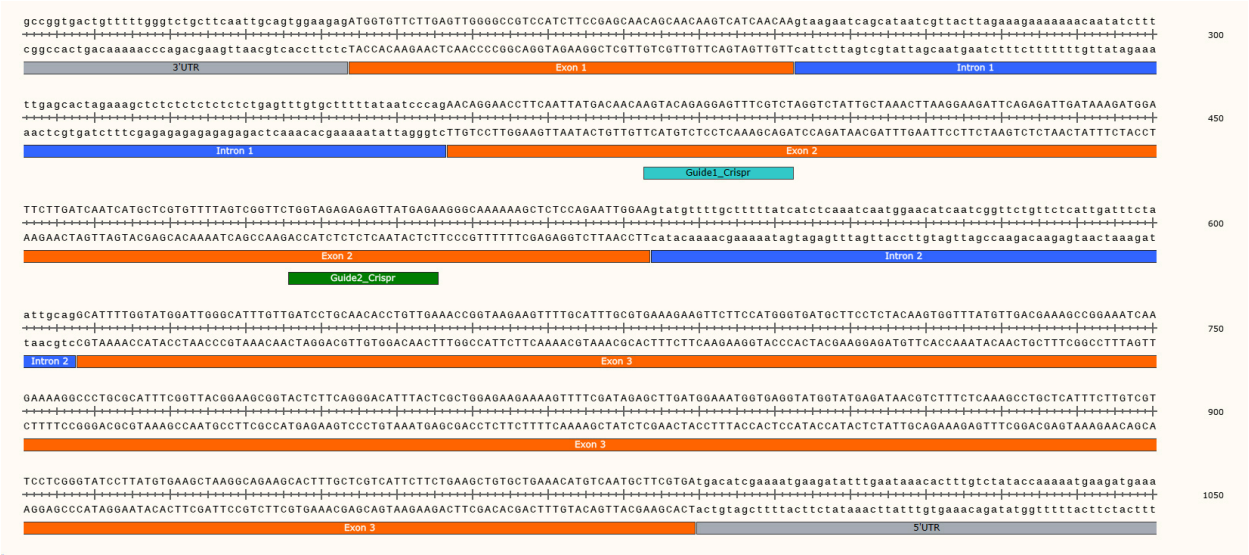

B

C

Supplemental Figure S2: clrp23 knock-out mutants generated with CRISPR/Cas9 technology A) gDNA sequence of *CLRP23*, and the two specific guide RNAs designed for CRISPR/Cas9 mutant knock-out. **B-C)** Confirmation of gene knock-out with PCR and Sanger Sequencing of mutant lines (A) *clrp23* and (B) *clrp23-2.* NCBI nucleotide BLAST was used to align the sequencing data with the gDNA sequence of *CLRP23.*

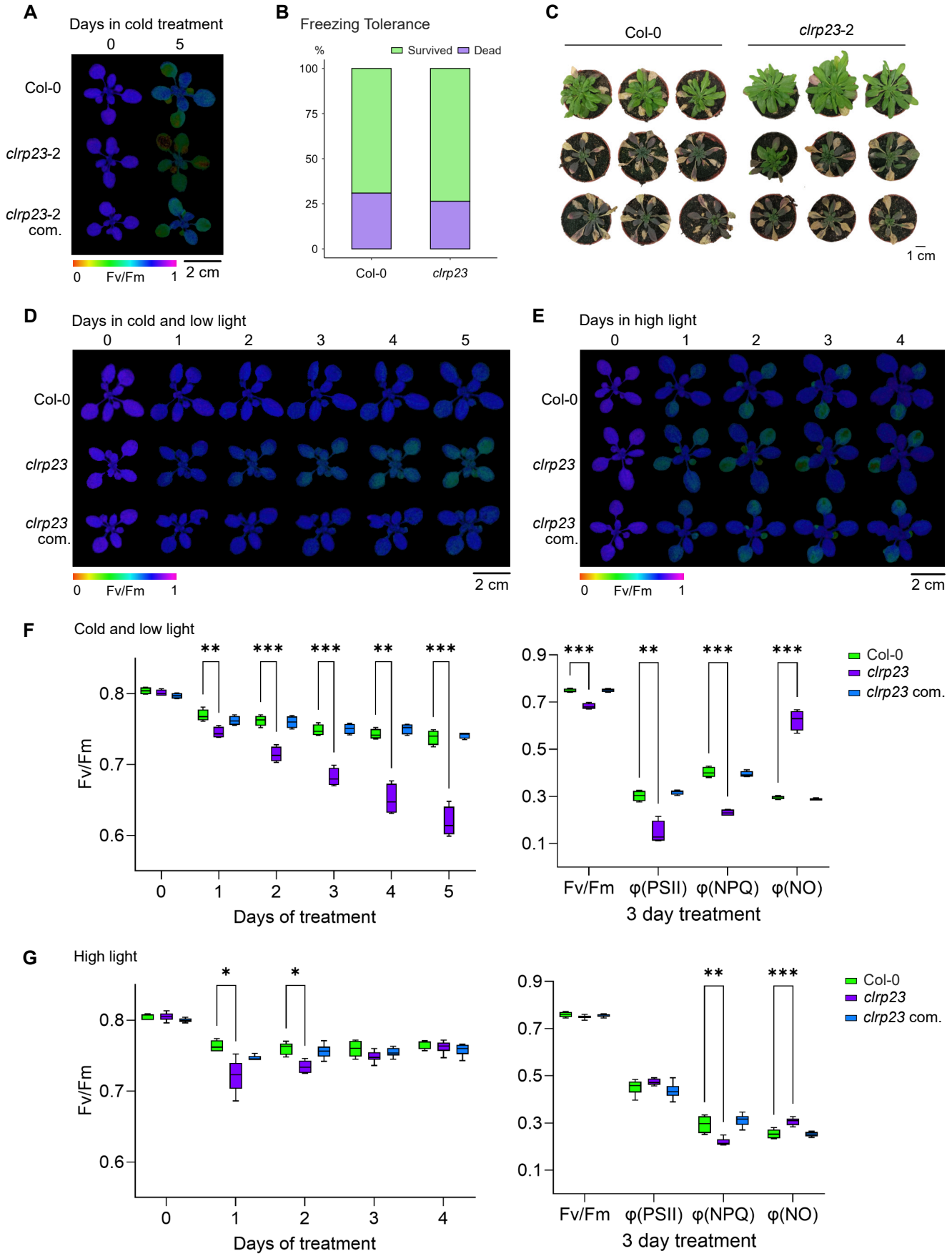

Supplemental Figure S3: *clrp23* mutants under cold, freezing, cold/low light and room temperature/high light conditions. A) Independent CRISPR mutant line lacking CLRP23, *clrp23-2* and the corresponding complementation line, *clrp23-2* com under cold treatment (4ºC, 250 µE, 16h light). **B-C)** Col-0 and *clrp23* plants were subjected to freezing treatment. (B) shows the survival rates of Col-0 and *clrp23* to freezing and (C) shows the representative diversity of plants responding to freezing treatment after recovery to 22ºC **D-G)** Col-0, *clrp23* and complemented plants were grown under standard growth conditions for 20 days before transferring to cold/low light (4ºC, 80 µE, 16h light) and room temperature/high light conditions (22ºC, 500 µE, 16h day/18ºC night). **D-E)** Chlorophyll fluorescence imaging during cold low light (D) and room temperature high light (E) treatment. **F-G)** Fv/Fm values after 0-5 days, as well as Fv/Fm, PSII quantum yield (φ(PSII)), non-photochemical quenching (φ(NPQ)) and nonregulated energy dissipation (φ(NO)) after 3 days of cold low light (F) and room temperature high light (G) treatment. Asterisks indicate statistically significant differences according to Student's t-test (*p<0.05; **p<0.01; ***p<0.001).

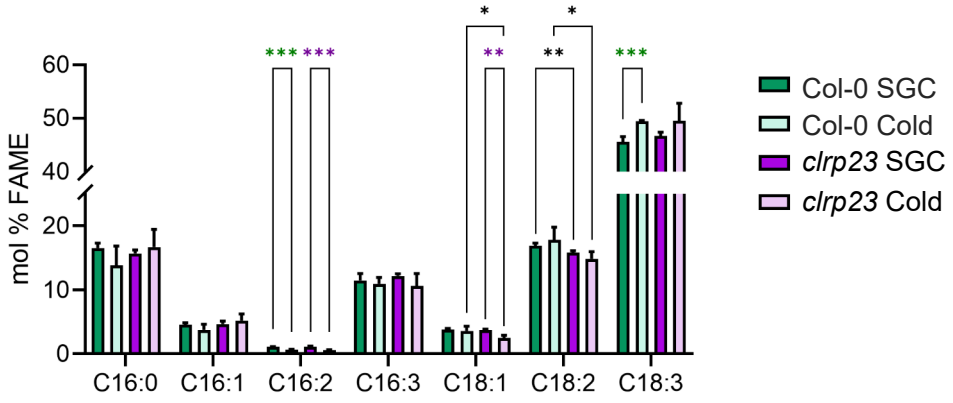

Supplemental Figure S4: Total lipid analysis of *clrp23* mutants under standard growth conditions (SGC) and after cold treatment. Fatty acids of total lipid extraction were quantified with GC-FID and reported as molar percentage (mol% FAME). Asterisks indicate statistically significant differences according to a Student's t-test (*p<0.05; **p<0.01; ***p<0.001).

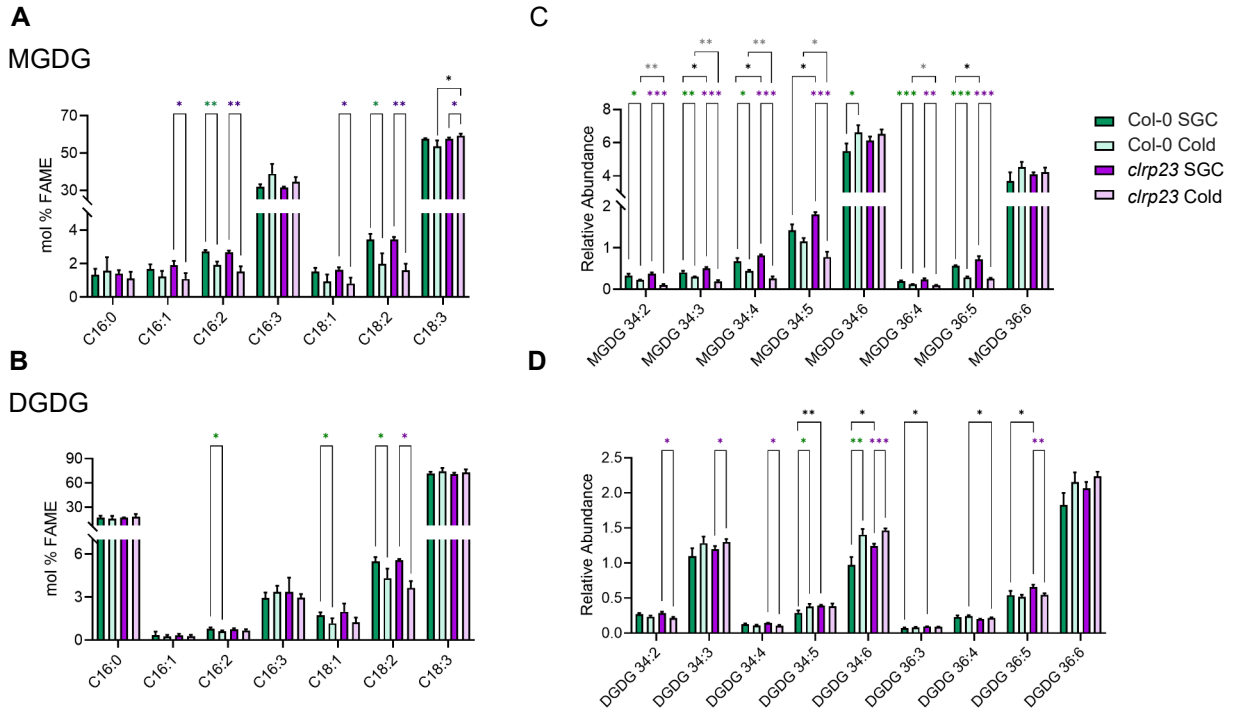

Supplemental Figure S5: Galactolipid analysis of *clrp23* mutants after cold treatment. Side by side comparison of MGDG (A, C) and DGDG (B, D) fatty acids (A-B) and lipid species (C-D) quantified with GC-FID and LC-MS, respectively. Fatty acids are reported as molar percentage (mol% FAME) and lipid species are reported as relative abundance (peak area relative to internal standard corticosterone). Asterisks indicate statistically significant differences according to a student t-test (*P<0.05; **P<0.01; ***P<0.001).

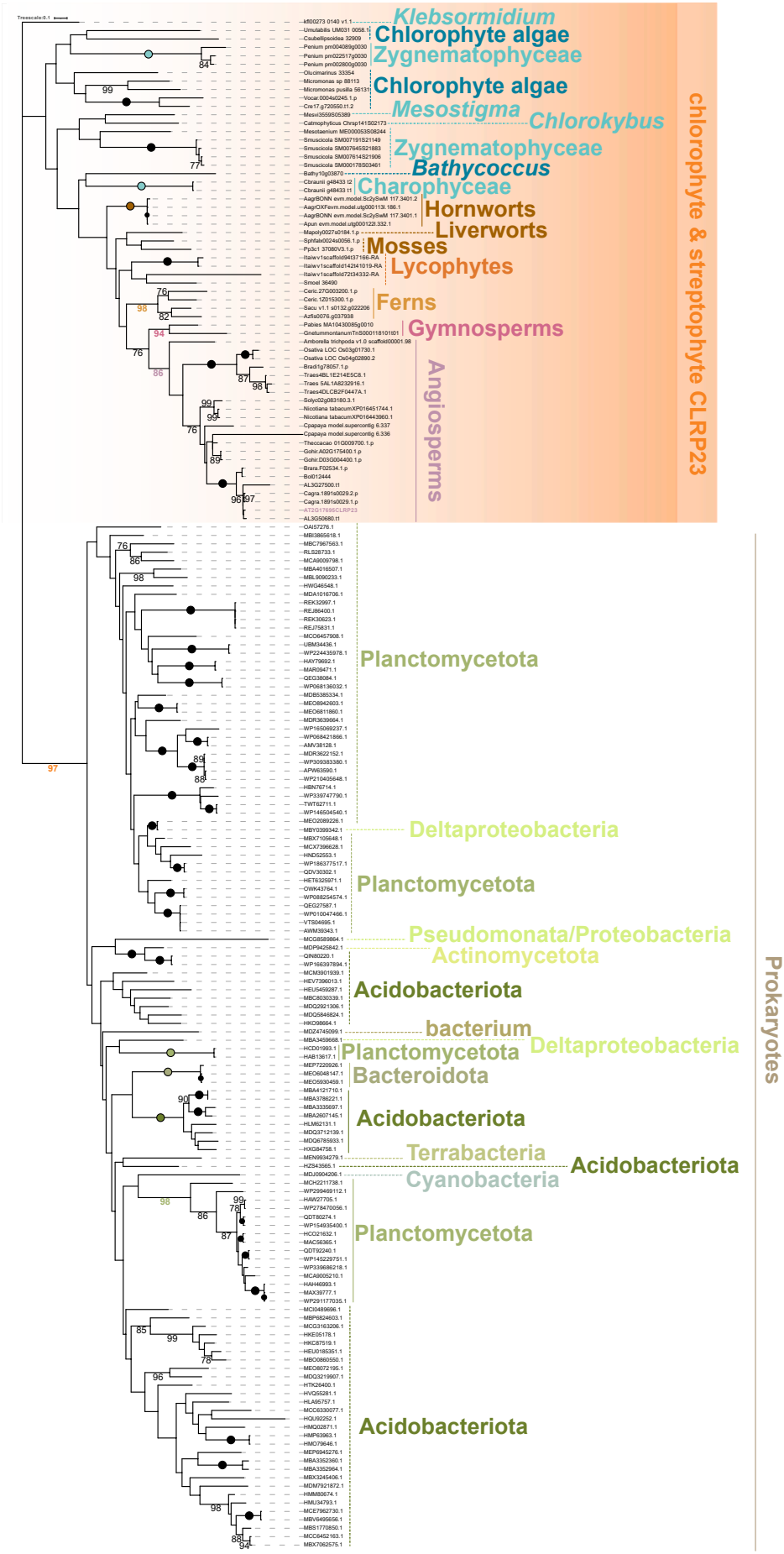

Supplemental Figure S6: Phylogenetic analyses of CLRP23. The unrooted phylogeny is based on BLASTp hits of *At*CLRP23 against a streptophyte and chlorophyte genome containing database and the nr database on ncbi restricted to (a) bacteria and (b) cyanobacteria. *Arabidopsis* gene family member CLRP23 is highlighted in light purple and bold. The CLRP23 sequences from Chloroplastida are highlighted by an orange box. Taxonomic affilication is indicated on the right. Bold lines show monophyletic groups with a minimum bootstrap support of >75. Dotted lines indicate sequences belonging to the same lineage, which are either paraphyletic or not supported to form a monophylum. Only bootstrap support of >75 is shown, bootstrap support of 100 is indicated by circles.

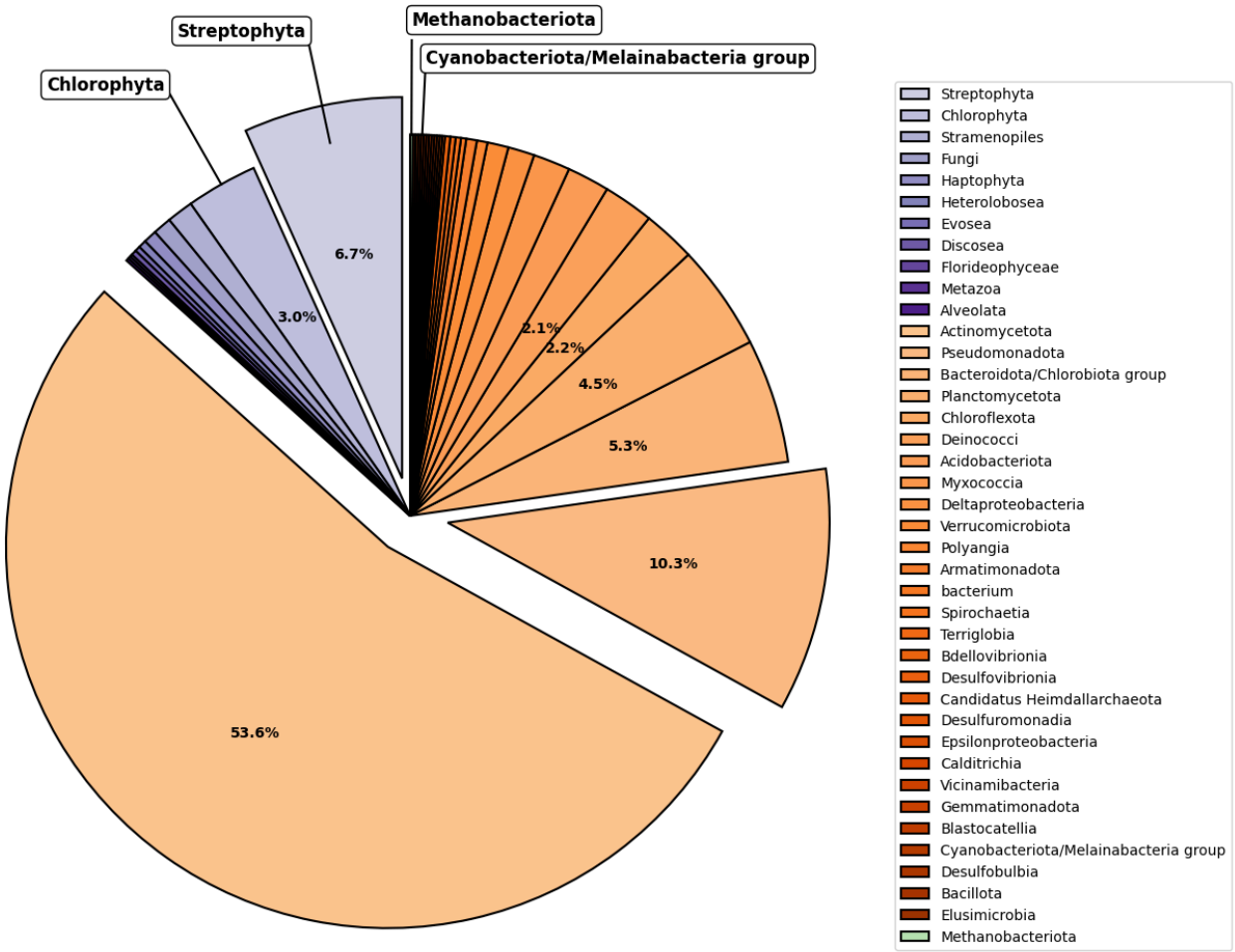

Supplemental Figure S7: Structural homologues of CLRP23. Taxonomic distribution of sequences that are structurally similar to *At*CLRP23, showing eukaryotes (blue), bacteria (orange and archae (green). Figure is based on results from Alphafold3 search in Table S6.

Supplementary Methods S1

Sequence homology and phylogenetic analysis

Protein data were downloaded from the genomes of *Anthoceros agrestis* Oxford and Bonn (Li et al., 2020), *Anthoceros punctatus* (Li et al., 2020), *Amborella trichopoda* (Amborella Genome Project et al., 2013), *A. thaliana* (Lamesch et al., 2011), *A. lyrata* (Hu et al., 2011), *Azolla filiculoides* (Li et al., 2018), *Bathycoccus prasinos* (Moreau et al., 2012), *Brassica oleracea* (Liu et al., 2014), *Brassica rapa* (Goodstein et al., 2011), *Brachypodium distachyon* (Vogel et al., 2010), *Capsella grandiflora* (Slotte et al., 2013), *Carica papaya* (Ming et al., 2008), *Ceratopteris richardii* (Marchant et al., 2022), *Chara braunii* (Nishiyama et al., 2018), *Chlorokybus melkonianii* ((Wang et al., 2020); for naming, see (Irisarri et al., 2021)), *Chlamydomonas reinhardtii* (Merchant et al., 2007), *Coccomyxa subellipsoidea* (Blanc et al., 2012), *Gnetum montanum* (Wan et al., 2018), *Gossypium hirsutum* (Li et al., 2015), *Isoetes taiwaniensis* (Wickell et al., 2021), *Klebsormidium nitens* (Hori et al., 2014), *M. polymorpha* (Bowman et al., 2017), *Mesostigma viride* (Wang et al., 2020), *Micromonas pusilla* (Worden et al., 2009), *Micromonas* sp. (Worden et al., 2009), *Nicotiana tabacum* (Sierro et al., 2014), *Oryza sativa* (Ouyang et al., 2006), *Picea abies* (Nystedt et al., 2013), *P. patens* (Lang et al., 2018a), *Salvinia cucullata* (Li et al., 2018), *Selaginella moellendorffii* (Banks et al., 2011), *Solanum lycopersicum* (Sato et al., 2012), *Sphagnum fallax* (Healey et al., 2023), *Theobroma cacao* (Argout et al., 2011), *Triticum aestivum* (The International Wheat Genome Sequencing Consortium et al., 2018), *Mesotaenium endlicherianum* V1 (Cheng et al., 2019), *Ostreococcus lucimarinus* (Palenik et al., 2007), *Penium margaritaceum* (Jiao et al., 2020), *Spirogloea muscicola* (Cheng et al., 2019), *Ulva mutabilis* (De Clerck et al., 2018), and *Volvox carteri* (Prochnik et al., 2010),).

For residue conservation comparison homologs of Arabidopsis CLRP23 were identified in Soybean (Schmutz et al., 2010), Tomato (Hosmani et al., 2019), Black cottonwood (Tuskan et al., 2006), Common grape vine (Jaillon et al., 2007), *Amborella trichopoda* (Amborella Genome Project, 2013), Rice (Ouyang et al., 2006), Maize (EnsemblPlants), *Selaginella moellendorffii* (Banks et al., 2011) and *Physcomitrium patens* (Lang et al., 2018b).

References

Amborella Genome Project, Albert, V.A., Barbazuk, W.B., dePamphilis, C.W., Der, J.P., Leebens-Mack, J., Ma, H., Palmer, J.D., Rounsley, S., Sankoff, D., Schuster, S.C., Soltis, D.E., Soltis, P.S., Wessler, S.R., Wing, R.A., Albert, V.A., Ammiraju, J.S.S., Barbazuk, W.B., Chamala, S., Chanderbali, A.S., dePamphilis, C.W., Der, J.P., Determann, R., Leebens-Mack, J., Ma, H., Ralph, P., Rounsley, S., Schuster, S.C., Soltis, D.E., Soltis, P.S., Talag, J., Tomsho, L., Walts, B., Wanke, S., Wing, R.A., Albert, V.A., Barbazuk, W.B., Chamala, S., Chanderbali, A.S., Chang, T.-H., Determann, R., Lan, T., Soltis, D.E., Soltis, P.S., Arikit, S., Axtell, M.J., Ayyampalayam, S., Barbazuk, W.B., Burnette, J.M., Chamala, S., De Paoli, E., dePamphilis, C.W., Der, J.P., Estill, J.C., Farrell, N.P., Harkess, A., Jiao, Y., Leebens-Mack, J., Liu, K., Mei, W., Meyers, B.C., Shahid, S., Wafula, E., Walts, B., Wessler, S.R., Zhai, J., Zhang, X., Albert, V.A., Carretero-Paulet, L., dePamphilis, C.W., Der, J.P., Jiao, Y., Leebens-Mack, J., Lyons, E., Sankoff, D., Tang, H., Wafula, E., Zheng, C., Albert, V.A., Altman, N.S., Barbazuk, W.B., Carretero-Paulet, L., dePamphilis, C.W., Der, J.P., Estill, J.C., Jiao, Y., Leebens-Mack, J., Liu, K., Mei, W., Wafula, E., Altman, N.S., Arikit, S., Axtell, M.J., Chamala, S., Chanderbali, A.S., Chen, F., Chen, J.-Q., Chiang, V., De Paoli, E., dePamphilis, C.W., Der, J.P., Determann, R., Fogliani, B., Guo, C., Harholt, J., Harkess, A., Job, C., Job, D., Kim, S., Kong, H., Leebens-Mack, J., Li, G., Li, L., Liu, J., Ma, H., Meyers, B.C., Park, J., Qi, X., Rajjou, L., Burtet-Sarramegna, V., Sederoff, R., Shahid, S., Soltis, D.E., Soltis, P.S., Sun, Y.-H., Ulvskov, P., Villegente, M., Xue, J.-Y., Yeh, T.-F., Yu, X., Zhai, J., Acosta, J.J., Albert, V.A., Barbazuk, W.B., Bruenn, R.A., Chamala, S., de Kochko, A., dePamphilis, C.W., Der, J.P., Herrera-Estrella, L.R., Ibarra-Laclette, E., Kirst, M., Leebens-Mack, J., Pissis, S.P., Poncet, V., Schuster, S.C., Soltis, D.E., Soltis, P.S., and Tomsho, L. (2013). The *Amborella* genome and the evolution of flowering plants. Science **342,** 1241089.

Argout, X., Salse, J., Aury, J.-M., Guiltinan, M.J., Droc, G., Gouzy, J., Allegre, M., Chaparro, C., Legavre, T., Maximova, S.N., Abrouk, M., Murat, F., Fouet, O., Poulain, J., Ruiz, M., Roguet, Y., Rodier-Goud, M., Barbosa-Neto, J.F., Sabot, F., Kudrna, D., Ammiraju, J.S.S., Schuster, S.C., Carlson, J.E., Sallet, E., Schiex, T., Dievart, A., Kramer, M., Gelley, L., Shi, Z., Bérard, A., Viot, C., Boccara, M., Risterucci, A.M., Guignon, V., Sabau, X., Axtell, M.J., Ma, Z., Zhang, Y., Brown, S., Bourge, M., Golser, W., Song, X., Clement, D., Rivallan, R., Tahi, M., Akaza, J.M., Pitollat, B., Gramacho, K., D'Hont, A., Brunel, D., Infante, D., Kebe, I., Costet, P., Wing, R., McCombie, W.R., Guiderdoni, E., Quetier, F., Panaud, O., Wincker, P., Bocs, S., and Lanaud, C. (2011). The genome of *Theobroma cacao*. Nature genetics **43,** 101-108.

Banks, J.A., Nishiyama, T., Hasebe, M., Bowman, J.L., Gribskov, M., dePamphilis, C., Albert, V.A., Aono, N., Aoyama, T., Ambrose, B.A., Ashton, N.W., Axtell, M.J., Barker, E., Barker, M.S., Bennetzen, J.L., Bonawitz, N.D., Chapple, C., Cheng, C., Correa, L.G.G., Dacre, M., DeBarry, J., Dreyer, I., Elias, M., Engstrom, E.M., Estelle, M., Feng, L., Finet, C., Floyd, S.K., Frommer, W.B., Fujita, T., Gramzow, L., Gutensohn, M., Harholt, J., Hattori, M., Heyl, A., Hirai, T., Hiwatashi, Y., Ishikawa, M., Iwata, M., Karol, K.G., Koehler, B., Kolukisaoglu, U., Kubo, M., Kurata, T., Lalonde, S., Li, K., Li, Y., Litt, A., Lyons, E., Manning, G., Maruyama, T., Michael, T.P., Mikami, K., Miyazaki, S., Morinaga, S.i., Murata, T., Mueller-Roeber, B., Nelson, D.R., Obara, M., Oguri, Y., Olmstead, R.G., Onodera, N., Petersen, B.L., Pils, B., Prigge, M., Rensing, S.A., Riaño-Pachón, D.M., Roberts, A.W., Sato, Y., Scheller, H.V., Schulz, B., Schulz, C., Shakirov, E.V., Shibagaki, N., Shinohara, N., Shippen, D.E., Sørensen, I., Sotooka, R., Sugimoto, N., Sugita, M., Sumikawa, N., Tanurdzic, M., Theißen, G., Ulvskov, P., Wakazuki, S., Weng, J.K., Willats, W.W.G.T., Wipf, D., Wolf, P.G., Yang, L., Zimmer, A.D., Zhu, Q., Mitros, T., Hellsten, U., Loqué, D., Otillar, R., Salamov, A., Schmutz, J., Shapiro,

H., Lindquist, E., Lucas, S., Rokhsar, D., and Grigoriev, I.V. (2011). The Selaginella Genome Identifies Genetic Changes Associated with the Evolution of Vascular Plants. Science **332,** 960-963.

Blanc, G., Agarkova, I., Grimwood, J., Kuo, A., Brueggeman, A., Dunigan, D.D., Gurnon, J., Ladunga, I., Lindquist, E., Lucas, S., Pangilinan, J., Pröschold, T., Salamov, A., Schmutz, J., Weeks, D., Yamada, T., Lomsadze, A., Borodovsky, M., Claverie, J.-M., Grigoriev, I.V., and Van Etten, J.L. (2012). The genome of the polar eukaryotic microalga *Coccomyxa subellipsoidea* reveals traits of cold adaptation. Genome Biol. **13,** R39.

Bowman, J.L., Kohchi, T., Yamato, K.T., Jenkins, J., Shu, S., Ishizaki, K., Yamaoka, S., Nishihama, R., Nakamura, Y., Berger, F., Adam, C., Aki, S.S., Althoff, F., Araki, T., Arteaga-Vazquez, M.A., Balasubrmanian, S., Barry, K., Bauer, D., Boehm, C.R., Briginshaw, L., Caballero-Perez, J., Catarino, B., Chen, F., Chiyoda, S., Chovatia, M., Davies, K.M., Delmans, M., Demura, T., Dierschke, T., Dolan, L., Dorantes-Acosta, A.E., Eklund, D.M., Florent, S.N., Flores-Sandoval, E., Fujiyama, A., Fukuzawa, H., Galik, B., Grimanelli, D., Grimwood, J., Grossniklaus, U., Hamada, T., Haseloff, J., Hetherington, A.J., Higo, A., Hirakawa, Y., Hundley, H.N., Ikeda, Y., Inoue, K., Inoue, S.-i., Ishida, S., Jia, Q., Kakita, M., Kanazawa, T., Kawai, Y., Kawashima, T., Kennedy, M., Kinose, K., Kinoshita, T., Kohara, Y., Koide, E., Komatsu, K., Kopischke, S., Kubo, M., Kyozuka, J., Lagercrantz, U., Lin, S.-S., Lindquist, E., Lipzen, A.M., Lu, C.-W., De Luna, E., Martienssen, R.A., Minamino, N., Mizutani, M., Mizutani, M., Mochizuki, N., Monte, I., Mosher, R., Nagasaki, H., Nakagami, H., Naramoto, S., Nishitani, K., Ohtani, M., Okamoto, T., Okumura, M., Phillips, J., Pollak, B., Reinders, A., Rövekamp, M., Sano, R., Sawa, S., Schmid, M.W., Shirakawa, M., Solano, R., Spunde, A., Suetsugu, N., Sugano, S., Sugiyama, A., Sun, R., Suzuki, Y., Takenaka, M., Takezawa, D., Tomogane, H., Tsuzuki, M., Ueda, T., Umeda, M., Ward, J.M., Watanabe, Y., Yazaki, K., Yokoyama, R., Yoshitake, Y., Yotsui, I., Zachgo, S., and Schmutz, J. (2017). Insights into land plant evolution garnered from the *Marchantia polymorpha* genome. Cell **171,** 287-304.e215.

Cheng, S., Xian, W., Fu, Y., Marin, B., Keller, J., Wu, T., Sun, W., Li, X., Xu, Y., Zhang, Y., Wittek, S., Reder, T., Günther, G., Gontcharov, A., Wang, S., Li, L., Liu, X., Wang, J., Yang, H., Xu, X., Delaux, P.-M., Melkonian, B., Wong, G.K.-S., and Melkonian, M. (2019). Genomes of subaerial Zygnematophyceae provide insights into land plant evolution. Cell **179,** 1057-1067.e1014.

De Clerck, O., Kao, S.-M., Bogaert, K.A., Blomme, J., Foflonker, F., Kwantes, M., Vancaester, E., Vanderstraeten, L., Aydogdu, E., Boesger, J., Califano, G., Charrier, B., Clewes, R., Del Cortona, A., D'Hondt, S., Fernandez-Pozo, N., Gachon, C.M., Hanikenne, M., Lattermann, L., Leliaert, F., Liu, X., Maggs, C.A., Popper, Z.A., Raven, J.A., Van Bel, M., Wilhelmsson, P.K.I., Bhattacharya, D., Coates, J.C., Rensing, S.A., Van Der Straeten, D., Vardi, A., Sterck, L., Vandepoele, K., Van de Peer, Y., Wichard, T., and Bothwell, J.H. (2018). Insights into the evolution of multicellularity from the sea lettuce genome. Curr. Biol. **28,** 2921-2933.e2925.

Goodstein, D.M., Shu, S., Howson, R., Neupane, R., Hayes, R.D., Fazo, J., Mitros, T., Dirks, W., Hellsten, U., Putnam, N., and Rokhsar, D.S. (2011). Phytozome: a comparative platform for green plant genomics. Nucleic Acids Research **40,** D1178-D1186.

Healey, A.L., Piatkowski, B., Lovell, J.T., Sreedasyam, A., Carey, S.B., Mamidi, S., Shu, S., Plott, C., Jenkins, J., Lawrence, T., Aguero, B., Carrell, A.A., Nieto-Lugilde, M., Talag, J., Duffy, A., Jawdy, S., Carter, K.R., Boston, L.B., Jones, T., Jaramillo-Chico, J., Harkess, A., Barry, K., Keymanesh, K., Bauer, D., Grimwood, J., Gunter, L., Schmutz, J., Weston, D.J., and Shaw, A.J. (2023). Newly identified sex chromosomes in the *Sphagnum* (peat moss) genome alter carbon sequestration and ecosystem dynamics. Nat. Plants **9,** 238-254.

Hori, K., Maruyama, F., Fujisawa, T., Togashi, T., Yamamoto, N., Seo, M., Sato, S., Yamada, T., Mori, H., Tajima, N., Moriyama, T., Ikeuchi, M., Watanabe, M., Wada, H., Kobayashi, K., Saito, M., Masuda, T., Sasaki-Sekimoto, Y., Mashiguchi, K., Awai, K., Shimojima, M., Masuda, S., Iwai, M., Nobusawa, T., Narise, T., Kondo, S., Saito, H., Sato, R., Murakawa, M., Ihara, Y., Oshima-Yamada, Y., Ohtaka, K., Satoh, M., Sonobe, K., Ishii, M., Ohtani, R., Kanamori-Sato, M., Honoki, R., Miyazaki, D., Mochizuki, H., Umetsu, J., Higashi, K., Shibata, D., Kamiya, Y., Sato, N., Nakamura, Y., Tabata, S., Ida, S., Kurokawa, K., and Ohta, H. (2014). *Klebsormidium flaccidum* genome reveals primary factors for plant terrestrial adaptation. Nat. Commun. **5,** 3978.

Hosmani, P.S., Flores-Gonzalez, M., van de Geest, H., Maumus, F., Bakker, L.V., Schijlen, E., van Haarst, J., Cordewener, J., Sanchez-Perez, G., and Peters, S. (2019). An improved de novo assembly and annotation of the tomato reference genome using single-molecule sequencing, Hi-C proximity ligation and optical maps. biorxiv, 767764.

Hu, T.T., Pattyn, P., Bakker, E.G., Cao, J., Cheng, J.F., Clark, R.M., Fahlgren, N., Fawcett, J.A., Grimwood, J., Gundlach, H., Haberer, G., Hollister, J.D., Ossowski, S., Ottilar, R.P., Salamov, A.A., Schneeberger, K., Spannagl, M., Wang, X., Yang, L., Nasrallah, M.E., Bergelson, J., Carrington, J.C., Gaut, B.S., Schmutz, J., Mayer, K.F., Van de Peer, Y., Grigoriev, I.V., Nordborg, M., Weigel, D., and Guo, Y.L. (2011). The *Arabidopsis lyrata* genome sequence and the basis of rapid genome size change. Nature genetics **43,** 476-481.

Irisarri, I., Darienko, T., Pröschold, T., Fürst-Jansen, J.M.R., Jamy, M., and de Vries, J. (2021). Unexpected cryptic species among streptophyte algae most distant to land plants. Proceedings of the Royal Society B: Biological Sciences **288,** 20212168.

Jaillon, O., Aury, J.-M., Noel, B., Policriti, A., Clepet, C., Casagrande, A., Choisne, N., Aubourg, S., Vitulo, N., Jubin, C., Vezzi, A., Legeai, F., Hugueney, P., Dasilva, C., Horner, D., Mica, E., Jublot, D., Poulain, J., Bruyère, C., Billault, A., Segurens, B., Gouyvenoux, M., Ugarte, E., Cattonaro, F., Anthouard, V., Vico, V., Del Fabbro, C., Alaux, M., Di Gaspero, G., Dumas, V., Felice, N., Paillard, S., Juman, I., Moroldo, M., Scalabrin, S., Canaguier, A., Le Clainche, I., Malacrida, G., Durand, E., Pesole, G., Laucou, V., Chatelet, P., Merdinoglu, D., Delledonne, M., Pezzotti, M., Lecharny, A., Scarpelli, C., Artiguenave, F., Pè, M.E., Valle, G., Morgante, M., Caboche, M., Adam-Blondon, A.-F., Weissenbach, J., Quétier, F., Wincker, P., and The French–Italian Public Consortium for Grapevine Genome, C. (2007). The grapevine genome sequence suggests ancestral hexaploidization in major angiosperm phyla. Nature **449,** 463-467.

Jiao, C., Sørensen, I., Sun, X., Sun, H., Behar, H., Alseekh, S., Philippe, G., Palacio Lopez, K., Sun, L., Reed, R., Jeon, S., Kiyonami, R., Zhang, S., Fernie, A.R., Brumer, H., Domozych, D.S., Fei, Z., and Rose, J.K.C. (2020). The *Penium margaritaceum* genome: Hallmarks of the origins of land plants. Cell **181,** 1097-1111.

Lamesch, P., Berardini, T.Z., Li, D., Swarbreck, D., Wilks, C., Sasidharan, R., Muller, R., Dreher, K., Alexander, D.L., Garcia-Hernandez, M., Karthikeyan, A.S., Lee, C.H., Nelson, W.D., Ploetz, L., Singh, S., Wensel, A., and Huala, E. (2011). The Arabidopsis Information Resource (TAIR): improved gene annotation and new tools. Nucleic Acids Res. **40,** D1202-D1210.

Lang, D., Ullrich, K.K., Murat, F., Fuchs, J., Jenkins, J., Haas, F.B., Piednoel, M., Gundlach, H., Van Bel, M., Meyberg, R., Vives, C., Morata, J., Symeonidi, A., Hiss, M., Muchero, W., Kamisugi, Y., Saleh, O., Blanc, G., Decker, E.L., van Gessel, N., Grimwood, J., Hayes, R.D., Graham, S.W., Gunter, L.E., McDaniel, S., Hoernstein, S.N.W., Larsson, A., Li, F.-W., Perroud, P.-F., Phillips, J., Ranjan, P., Rokshar, D.S., Rothfels, C.J., Schneider, L., Shu, S., Stevenson, D.W., Thümmler, F., Tillich, M., Villarreal A, J.C., Widiez, T., Wong, G.K.-S., Wymore, A., Zhang, Y., Zimmer, A.D., Quatrano, R.S., Mayer, K.F.X., Goodstein, D., Casacuberta, J.M., Vandepoele, K., Reski, R., Cuming, A.C., Tuskan, J., Maumus, F., Salse, J., Schmutz, J., and Rensing, S.A. (2018a). The *Physcomitrella*

patens chromosome-scale assembly reveals moss genome structure and evolution. Plant J. **93,** 515-533.

Lang, D., Ullrich, K.K., Murat, F., Fuchs, J., Jenkins, J., Haas, F.B., Piednoel, M., Gundlach, H., Van Bel, M., Meyberg, R., Vives, C., Morata, J., Symeonidi, A., Hiss, M., Muchero, W., Kamisugi, Y., Saleh, O., Blanc, G., Decker, E.L., van Gessel, N., Grimwood, J., Hayes, R.D., Graham, S.W., Gunter, L.E., McDaniel, S.F., Hoernstein, S.N.W., Larsson, A., Li, F.-W., Perroud, P.-F., Phillips, J., Ranjan, P., Rokshar, D.S., Rothfels, C.J., Schneider, L., Shu, S., Stevenson, D.W., Thümmler, F., Tillich, M., Villarreal Aguilar, J.C., Widiez, T., Wong, G.K.-S., Wymore, A., Zhang, Y., Zimmer, A.D., Quatrano, R.S., Mayer, K.F.X., Goodstein, D., Casacuberta, J.M., Vandepoele, K., Reski, R., Cuming, A.C., Tuskan, G.A., Maumus, F., Salse, J., Schmutz, J., and Rensing, S.A. (2018b). The Physcomitrella patens chromosome-scale assembly reveals moss genome structure and evolution. The Plant Journal **93,** 515-533.

Li, F.-W., Nishiyama, T., Waller, M., Frangedakis, E., Keller, J., Li, Z., Fernandez-Pozo, N., Barker, M.S., Bennett, T., Blázquez, M.A., Cheng, S., Cuming, A.C., de Vries, J., de Vries, S., Delaux, P.-M., Diop, I.S., Harrison, C.J., Hauser, D., Hernández-García, J., Kirbis, A., Meeks, J.C., Monte, I., Mutte, S.K., Neubauer, A., Quandt, D., Robison, T., Shimamura, M., Rensing, S.A., Villarreal, J.C., Weijers, D., Wicke, S., Wong, G.K.S., Sakakibara, K., and Szövényi, P. (2020). *Anthoceros* genomes illuminate the origin of land plants and the unique biology of hornworts. Nat. Plants **6,** 259-272.

Li, F.-W., Brouwer, P., Carretero-Paulet, L., Cheng, S., de Vries, J., Delaux, P.-M., Eily, A., Koppers, N., Kuo, L.-Y., Li, Z., Simenc, M., Small, I., Wafula, E., Angarita, S., Barker, M.S., Bräutigam, A., dePamphilis, C., Gould, S., Hosmani, P.S., Huang, Y.-M., Huettel, B., Kato, Y., Liu, X., Maere, S., McDowell, R., Mueller, L.A., Nierop, K.G.J., Rensing, S.A., Robison, T., Rothfels, C.J., Sigel, E.M., Song, Y., Timilsena, P.R., Van de Peer, Y., Wang, H., Wilhelmsson, P.K.I., Wolf, P.G., Xu, X., Der, J.P., Schluepmann, H., Wong, G.K.S., and Pryer, K.M. (2018). Fern genomes elucidate land plant evolution and cyanobacterial symbioses. Nat. Plants **4,** 460-472.

Li, F., Fan, G., Lu, C., Xiao, G., Zou, C., Kohel, R.J., Ma, Z., Shang, H., Ma, X., Wu, J., Liang, X., Huang, G., Percy, R.G., Liu, K., Yang, W., Chen, W., Du, X., Shi, C., Yuan, Y., Ye, W., Liu, X., Zhang, X., Liu, W., Wei, H., Wei, S., Huang, G., Zhang, X., Zhu, S., Zhang, H., Sun, F., Wang, X., Liang, J., Wang, J., He, Q., Huang, L., Wang, J., Cui, J., Song, G., Wang, K., Xu, X., Yu, J.Z., Zhu, Y., and Yu, S. (2015). Genome sequence of cultivated Upland cotton (*Gossypium hirsutum* TM-1) provides insights into genome evolution. Nature Biotechnol. **33,** 524-530.

Liu, S., Liu, Y., Yang, X., Tong, C., Edwards, D., Parkin, I.A.P., Zhao, M., Ma, J., Yu, J., Huang, S., Wang, X., Wang, J., Lu, K., Fang, Z., Bancroft, I., Yang, T.-J., Hu, Q., Wang, X., Yue, Z., Li, H., Yang, L., Wu, J., Zhou, Q., Wang, W., King, G.J., Pires, J.C., Lu, C., Wu, Z., Sampath, P., Wang, Z., Guo, H., Pan, S., Yang, L., Min, J., Zhang, D., Jin, D., Li, W., Belcram, H., Tu, J., Guan, M., Qi, C., Du, D., Li, J., Jiang, L., Batley, J., Sharpe, A.G., Park, B.-S., Ruperao, P., Cheng, F., Waminal, N.E., Huang, Y., Dong, C., Wang, L., Li, J., Hu, Z., Zhuang, M., Huang, Y., Huang, J., Shi, J., Mei, D., Liu, J., Lee, T.-H., Wang, J., Jin, H., Li, Z., Li, X., Zhang, J., Xiao, L., Zhou, Y., Liu, Z., Liu, X., Qin, R., Tang, X., Liu, W., Wang, Y., Zhang, Y., Lee, J., Kim, H.H., Denoeud, F., Xu, X., Liang, X., Hua, W., Wang, X., Wang, J., Chalhoub, B., and Paterson, A.H. (2014). The *Brassica oleracea* genome reveals the asymmetrical evolution of polyploid genomes. Nat. Commun. **5,** 3930.

Marchant, D.B., Chen, G., Cai, S., Chen, F., Schafran, P., Jenkins, J., Shu, S., Plott, C., Webber, J., Lovell, J.T., He, G., Sandor, L., Williams, M., Rajasekar, S., Healey, A., Barry, K., Zhang, Y., Sessa, E., Dhakal, R.R., Wolf, P.G., Harkess, A., Li, F.-W., Rössner, C., Becker, A., Gramzow, L., Xue, D., Wu, Y., Tong, T., Wang, Y., Dai, F., Hua, S., Wang, H., Xu, S., Xu, F., Duan, H., Theißen, G., McKain, M.R., Li, Z., McKibben, M.T.W., Barker, M.S., Schmitz, R.J., Stevenson, D.W., Zumajo-Cardona, C., Ambrose, B.A., Leebens-Mack, J.H., Grimwood, J., Schmutz, J.,

Soltis, P.S., Soltis, D.E., and Chen, Z.-H. (2022). Dynamic genome evolution in a model fern. Nat. Plants **8,** 1038-1051.

Merchant, S.S., Prochnik, S.E., Vallon, O., Harris, E.H., Karpowicz, S.J., Witman, G.B., Terry, A., Salamov, A., Fritz-Laylin, L.K., Marechal-Drouard, L., Marshall, W.F., Qu, L.H., Nelson, D.R., Sanderfoot, A.A., Spalding, M.H., Kapitonov, V.V., Ren, Q., Ferris, P., Lindquist, E., Shapiro, H., Lucas, S.M., Grimwood, J., Schmutz, J., Cardol, P., Cerutti, H., Chanfreau, G., Chen, C.L., Cognat, V., Croft, M.T., Dent, R., Dutcher, S., Fernandez, E., Fukuzawa, H., Gonzalez-Ballester, D., Gonzalez-Halphen, D., Hallmann, A., Hanikenne, M., Hippler, M., Inwood, W., Jabbari, K., Kalanon, M., Kuras, R., Lefebvre, P.A., Lemaire, S.D., Lobanov, A.V., Lohr, M., Manuell, A., Meier, I., Mets, L., Mittag, M., Mittelmeier, T., Moroney, J.V., Moseley, J., Napoli, C., Nedelcu, A.M., Niyogi, K., Novoselov, S.V., Paulsen, I.T., Pazour, G., Purton, S., Ral, J.P., Riano-Pachon, D.M., Riekhof, W., Rymarquis, L., Schroda, M., Stern, D., Umen, J., Willows, R., Wilson, N., Zimmer, S.L., Allmer, J., Balk, J., Bisova, K., Chen, C.J., Elias, M., Gendler, K., Hauser, C., Lamb, M.R., Ledford, H., Long, J.C., Minagawa, J., Page, M.D., Pan, J., Pootakham, W., Roje, S., Rose, A., Stahlberg, E., Terauchi, A.M., Yang, P., Ball, S., Bowler, C., Dieckmann, C.L., Gladyshev, V.N., Green, P., Jorgensen, R., Mayfield, S., Mueller-Roeber, B., Rajamani, S., Sayre, R.T., Brokstein, P., Dubchak, I., Goodstein, D., Hornick, L., Huang, Y.W., Jhaveri, J., Luo, Y., Martinez, D., Ngau, W.C., Otillar, B., Poliakov, A., Porter, A., Szajkowski, L., Werner, G., Zhou, K., Grigoriev, I.V., Rokhsar, D.S., and Grossman, A.R. (2007). The *Chlamydomonas* genome reveals the evolution of key animal and plant functions. Science **318,** 245-250.

Ming, R., Hou, S., Feng, Y., Yu, Q., Dionne-Laporte, A., Saw, J.H., Senin, P., Wang, W., Ly, B.V., Lewis, K.L., Salzberg, S.L., Feng, L., Jones, M.R., Skelton, R.L., Murray, J.E., Chen, C., Qian, W., Shen, J., Du, P., Eustice, M., Tong, E., Tang, H., Lyons, E., Paull, R.E., Michael, T.P., Wall, K., Rice, D.W., Albert, H., Wang, M.L., Zhu, Y.J., Schatz, M., Nagarajan, N., Acob, R.A., Guan, P., Blas, A., Wai, C.M., Ackerman, C.M., Ren, Y., Liu, C., Wang, J., Wang, J., Na, J.K., Shakirov, E.V., Haas, B., Thimmapuram, J., Nelson, D., Wang, X., Bowers, J.E., Gschwend, A.R., Delcher, A.L., Singh, R., Suzuki, J.Y., Tripathi, S., Neupane, K., Wei, H., Irikura, B., Paidi, M., Jiang, N., Zhang, W., Presting, G., Windsor, A., Navajas-Perez, R., Torres, M.J., Feltus, F.A., Porter, B., Li, Y., Burroughs, A.M., Luo, M.C., Liu, L., Christopher, D.A., Mount, S.M., Moore, P.H., Sugimura, T., Jiang, J., Schuler, M.A., Friedman, V., Mitchell-Olds, T., Shippen, D.E., dePamphilis, C.W., Palmer, J.D., Freeling, M., Paterson, A.H., Gonsalves, D., Wang, L., and Alam, M. (2008). The draft genome of the transgenic tropical fruit tree papaya (*Carica papaya* Linnaeus). Nature **452,** 991-996.

Moreau, H., Verhelst, B., Couloux, A., Derelle, E., Rombauts, S., Grimsley, N., Van Bel, M., Poulain, J., Katinka, M., Hohmann-Marriott, M.F., Piganeau, G., Rouzé, P., Da Silva, C., Wincker, P., Van de Peer, Y., and Vandepoele, K. (2012). Gene functionalities and genome structure in *Bathycoccus prasinos* reflect cellular specializations at the base of the green lineage. Genome Biol. **13,** R74.

Nishiyama, T., Sakayama, H., de Vries, J., Buschmann, H., Saint-Marcoux, D., Ullrich, K.K., Haas, F.B., Vanderstraeten, L., Becker, D., Lang, D., Vosolsobě, S., Rombauts, S., Wilhelmsson, P.K.I., Janitza, P., Kern, R., Heyl, A., Rümpler, F., Villalobos, L.I.A.C., Clay, J.M., Skokan, R., Toyoda, A., Suzuki, Y., Kagoshima, H., Schijlen, E., Tajeshwar, N., Catarino, B., Hetherington, A.J., Saltykova, A., Bonnot, C., Breuninger, H., Symeonidi, A., Radhakrishnan, G.V., Van Nieuwerburgh, F., Deforce, D., Chang, C., Karol, K.G., Hedrich, R., Ulvskov, P., Glöckner, G., Delwiche, C.F., Petrášek, J., Van de Peer, Y., Friml, J., Beilby, M., Dolan, L., Kohara, Y., Sugano, S., Fujiyama, A., Delaux, P.-M., Quint, M., Theißen, G., Hagemann, M., Harholt, J., Dunand, C., Zachgo, S., Langdale, J., Maumus, F., Van Der Straeten, D., Gould, S.B., and Rensing, S.A. (2018). The *Chara* genome: Secondary complexity and implications for plant terrestrialization. Cell **174,** 448-464.

Nystedt, B., Street, N.R., Wetterbom, A., Zuccolo, A., Lin, Y.-C., Scofield, D.G., Vezzi, F., Delhomme, N., Giacomello, S., Alexeyenko, A., Vicedomini, R., Sahlin, K., Sherwood, E., Elfstrand, M., Gramzow, L., Holmberg, K., Hällman, J., Keech, O., Klasson, L., Koriabine, M., Kucukoglu, M., Käller, M., Luthman, J., Lysholm, F., Niittylä, T., Olson, Å., Rilakovic, N., Ritland, C., Rosselló, J.A., Sena, J., Svensson, T., Talavera-López, C., Theißen, G., Tuominen, H., Vanneste, K., Wu, Z.-Q., Zhang, B., Zerbe, P., Arvestad, L., Bhalerao, R., Bohlmann, J., Bousquet, J., Garcia Gil, R., Hvidsten, T.R., de Jong, P., MacKay, J., Morgante, M., Ritland, K., Sundberg, B., Lee Thompson, S., Van de Peer, Y., Andersson, B., Nilsson, O., Ingvarsson, P.K., Lundeberg, J., and Jansson, S. (2013). The Norway spruce genome sequence and conifer genome evolution. Nature **497,** 579-584.

Ouyang, S., Zhu, W., Hamilton, J., Lin, H., Campbell, M., Childs, K., Thibaud-Nissen, F., Malek, R.L., Lee, Y., Zheng, L., Orvis, J., Haas, B., Wortman, J., and Buell, C.R. (2006). The TIGR Rice Genome Annotation Resource: improvements and new features. Nucleic Acids Research **35,** D883-D887.

Palenik, B., Grimwood, J., Aerts, A., Rouze, P., Salamov, A., Putnam, N., Dupont, C., Jorgensen, R., Derelle, E., Rombauts, S., Zhou, K., Otillar, R., Merchant, S.S., Podell, S., Gaasterland, T., Napoli, C., Gendler, K., Manuell, A., Tai, V., Vallon, O., Piganeau, G., Jancek, S., Heijde, M., Jabbari, K., Bowler, C., Lohr, M., Robbens, S., Werner, G., Dubchak, I., Pazour, G.J., Ren, Q., Paulsen, I., Delwiche, C., Schmutz, J., Rokhsar, D., Van de Peer, Y., Moreau, H., and Grigoriev, I.V. (2007). The tiny eukaryote *Ostreococcus* provides genomic insights into the paradox of plankton speciation. PNAS **104,** 7705-7710.

Prochnik, S.E., Umen, J., Nedelcu, A.M., Hallmann, A., Miller, S.M., Nishii, I., Ferris, P., Kuo, A., Mitros, T., Fritz-Laylin, L.K., Hellsten, U., Chapman, J., Simakov, O., Rensing, S.A., Terry, A., Pangilinan, J., Kapitonov, V., Jurka, J., Salamov, A., Shapiro, H., Schmutz, J., Grimwood, J., Lindquist, E., Lucas, S., Grigoriev, I.V., Schmitt, R., Kirk, D., and Rokhsar, D.S. (2010). Genomic analysis of organismal complexity in the multicellular green alga *Volvox carteri*. Science **329,** 223-226.

Project, A.G., Albert, V.A., Barbazuk, W.B., dePamphilis, C.W., Der, J.P., Leebens-Mack, J., Ma, H., Palmer, J.D., Rounsley, S., Sankoff, D., Schuster, S.C., Soltis, D.E., Soltis, P.S., Wessler, S.R., Wing, R.A., Albert, V.A., Ammiraju, J.S.S., Barbazuk, W.B., Chamala, S., Chanderbali, A.S., dePamphilis, C.W., Der, J.P., Determann, R., Leebens-Mack, J., Ma, H., Ralph, P., Rounsley, S., Schuster, S.C., Soltis, D.E., Soltis, P.S., Talag, J., Tomsho, L., Walts, B., Wanke, S., Wing, R.A., Albert, V.A., Barbazuk, W.B., Chamala, S., Chanderbali, A.S., Chang, T.-H., Determann, R., Lan, T., Soltis, D.E., Soltis, P.S., Arikit, S., Axtell, M.J., Ayyampalayam, S., Barbazuk, W.B., Burnette, J.M., Chamala, S., De Paoli, E., dePamphilis, C.W., Der, J.P., Estill, J.C., Farrell, N.P., Harkess, A., Jiao, Y., Leebens-Mack, J., Liu, K., Mei, W., Meyers, B.C., Shahid, S., Wafula, E., Walts, B., Wessler, S.R., Zhai, J., Zhang, X., Albert, V.A., Carretero-Paulet, L., dePamphilis, C.W., Der, J.P., Jiao, Y., Leebens-Mack, J., Lyons, E., Sankoff, D., Tang, H., Wafula, E., Zheng, C., Albert, V.A., Altman, N.S., Barbazuk, W.B., Carretero-Paulet, L., dePamphilis, C.W., Der, J.P., Estill, J.C., Jiao, Y., Leebens-Mack, J., Liu, K., Mei, W., Wafula, E., Altman, N.S., Arikit, S., Axtell, M.J., Chamala, S., Chanderbali, A.S., Chen, F., Chen, J.-Q., Chiang, V., De Paoli, E., dePamphilis, C.W., Der, J.P., Determann, R., Fogliani, B., Guo, C., Harholt, J., Harkess, A., Job, C., Job, D., Kim, S., Kong, H., Leebens-Mack, J., Li, G., Li, L., Liu, J., Ma, H., Meyers, B.C., Park, J., Qi, X., Rajjou, L., Burtet-Sarramegna, V., Sederoff, R., Shahid, S., Soltis, D.E., Soltis, P.S., Sun, Y.-H., Ulvskov, P., Villegente, M., Xue, J.-Y., Yeh, T.-F., Yu, X., Zhai, J., Acosta, J.J., Albert, V.A., Barbazuk, W.B., Bruenn, R.A., Chamala, S., de Kochko, A., dePamphilis, C.W., Der, J.P., Herrera-Estrella, L.R., Ibarra-Laclette, E., Kirst, M., Leebens-Mack, J., Pissis, S.P., Poncet, V., Schuster, S.C., Soltis, D.E., Soltis, P.S., and Tomsho, L. (2013). The Amborella Genome and the Evolution of Flowering Plants. Science **342,** 1241089.

Sato, S., Tabata, S., Hirakawa, H., Asamizu, E., Shirasawa, K., Isobe, S., Kaneko, T., Nakamura, Y., Shibata, D., Aoki, K., Egholm, M., Knight, J., Bogden, R., Li, C., Shuang, Y., Xu, X., Pan, S., Cheng, S., Liu, X., Ren, Y., Wang, J., Albiero, A., Dal Pero, F., Todesco, S., Van Eck, J., Buels, R.M., Bombarely, A., Gosselin, J.R., Huang, M., Leto, J.A., Menda, N., Strickler, S., Mao, L., Gao, S., Tecle, I.Y., York, T., Zheng, Y., Vrebalov, J.T., Lee, J., Zhong, S., Mueller, L.A., Stiekema, W.J., Ribeca, P., Alioto, T., Yang, W., Huang, S., Du, Y., Zhang, Z., Gao, J., Guo, Y., Wang, X., Li, Y., He, J., Li, C., Cheng, Z., Zuo, J., Ren, J., Zhao, J., Yan, L., Jiang, H., Wang, B., Li, H., Li, Z., Fu, F., Chen, B., Han, B., Feng, Q., Fan, D., Wang, Y., Ling, H., Xue, Y., Ware, D., Richard McCombie, W., Lippman, Z.B., Chia, J.-M., Jiang, K., Pasternak, S., Gelley, L., Kramer, M., Anderson, L.K., Chang, S.-B., Royer, S.M., Shearer, L.A., Stack, S.M., Rose, J.K.C., Xu, Y., Eannetta, N., Matas, A.J., McQuinn, R., Tanksley, S.D., Camara, F., Guigó, R., Rombauts, S., Fawcett, J., Van de Peer, Y., Zamir, D., Liang, C., Spannagl, M., Gundlach, H., Bruggmann, R., Mayer, K., Jia, Z., Zhang, J., Ye, Z., Bishop, G.J., Butcher, S., Lopez-Cobollo, R., Buchan, D., Filippis, I., Abbott, J., Dixit, R., Singh, M., Singh, A., Kumar Pal, J., Pandit, A., Kumar Singh, P., Kumar Mahato, A., Dogra, V., Gaikwad, K., Raj Sharma, T., Mohapatra, T., Kumar Singh, N., Causse, M., Rothan, C., Schiex, T., Noirot, C., Bellec, A., Klopp, C., Delalande, C., Berges, H., Mariette, J., Frasse, P., Vautrin, S., Zouine, M., Latché, A., Rousseau, C., Regad, F., Pech, J.-C., Philippot, M., Bouzayen, M., Pericard, P., Osorio, S., Fernandez del Carmen, A., Monforte, A., Granell, A., Fernandez-Muñoz, R., Conte, M., Lichtenstein, G., Carrari, F., De Bellis, G., Fuligni, F., Peano, C., Grandillo, S., Termolino, P., Pietrella, M., Fantini, E., Falcone, G., Fiore, A., Giuliano, G., Lopez, L., Facella, P., Perrotta, G., Daddiego, L., Bryan, G., Orozco, M., Pastor, X., Torrents, D., van Schriek, M.G.M., Feron, R.M.C., van Oeveren, J., de Heer, P., daPonte, L., Jacobs-Oomen, S., Cariaso, M., Prins, M., van Eijk, M.J.T., Janssen, A., van Haaren, M.J.J., Jo, S.-H., Kim, J., Kwon, S.-Y., Kim, S., Koo, D.-H., Lee, S., Hur, C.-G., Clouser, C., Rico, A., Hallab, A., Gebhardt, C., Klee, K., Jöcker, A., Warfsmann, J., Göbel, U., Kawamura, S., Yano, K., Sherman, J.D., Fukuoka, H., Negoro, S., Bhutty, S., Chowdhury, P., Chattopadhyay, D., Datema, E., Smit, S., Schijlen, E.G.W.M., van de Belt, J., van Haarst, J.C., Peters, S.A., van Staveren, M.J., Henkens, M.H.C., Mooyman, P.J.W., Hesselink, T., van Ham, R.C.H.J., Jiang, G., Droege, M., Choi, D., Kang, B.-C., Dong Kim, B., Park, M., Kim, S., Yeom, S.-I., Lee, Y.-H., Choi, Y.-D., Li, G., Gao, J., Liu, Y., Huang, S., Fernandez-Pedrosa, V., Collado, C., Zuñiga, S., Wang, G., Cade, R., Dietrich, R.A., Rogers, J., Knapp, S., Fei, Z., White, R.A., Thannhauser, T.W., Giovannoni, J.J., Angel Botella, M., Gilbert, L., Gonzalez, R., The Tomato Genome, C., Kazusa, D.N.A.R.I., Life Sciences, a.R.c., Amplicon Express, I., Beijing Academy of, A., Forestry, S., Shenzhen, B.G.I., SrL, B.M.-G., Boyce Thompson Institute for Plant, R., Centre for BioSystems, G., Centro Nacional de Análisis, G., China Agricultural, U., Chinese Academy of Agricultural, S., Chinese Academy of, S., Cold Spring Harbor, L., United States Department of Agriculture – Agricultural Research, S., Colorado State, U., Cornell, U., Genome Bioinformatics Laboratory, G.I.U.P.F.C.R.G., Ghent University, V.I.B., Hebrew University of, J., Heilongjiang Academy of Agricultural, S., Helmholtz Center for, H., Environment, Henan Agricultural, U., Huazhong Agricultural, U., Imperial College, L., Indian Agricultural Research, I., Avignon, I., Bordeaux, I., Toulouse, I., Institut National Polytechnique de, T., Instituto de Biología Molecular y Celular de, P., Instituto de Hortofruticultura Subtropical y, M., Instituto Nacional de Tecnología, A., Consejo Nacionalde Investigaciones Científicas y, T., Italian National Res Council, I.f.B.T., Italian National Research Council, I.o.P.G.R.D.P., Italian National Agency for New technologies, E., Sustainable, D., James Hutton, I., Joint, I.R.B.B.S.C.p.o.C.B., Keygene, N.V., Korea Research Institute of, B., Biotechnology, Life, T., Max Planck Institute for Plant Breeding, R., Meiji, U., Montana State, U., Vegetable, N.I.o., Tea, S., National Institute of Plant

Genome, R., Plant Research, I., Qingdao Agricultural, U., Roche Applied, S., Seoul National, U., Shandong Academy of Agricultural, S., Sichuan, U., Sistemas, G., South China Agricultural, U., Syngenta, B., The Genome Analysis, C., The Natural History, M., United States Department of Agriculture – Agricultural Research Service, R.W.H.C., Boyce Thompson Institute for Plant, R., Universidad de Malaga-Consejo Superior de Investigaciones, C., and Universitat Pompeu, F. (2012). The tomato genome sequence provides insights into fleshy fruit evolution. Nature **485,** 635-641.

Schmutz, J., Cannon, S.B., Schlueter, J., Ma, J., Mitros, T., Nelson, W., Hyten, D.L., Song, Q., Thelen, J.J., Cheng, J., Xu, D., Hellsten, U., May, G.D., Yu, Y., Sakurai, T., Umezawa, T., Bhattacharyya, M.K., Sandhu, D., Valliyodan, B., Lindquist, E., Peto, M., Grant, D., Shu, S., Goodstein, D., Barry, K., Futrell-Griggs, M., Abernathy, B., Du, J., Tian, Z., Zhu, L., Gill, N., Joshi, T., Libault, M., Sethuraman, A., Zhang, X.-C., Shinozaki, K., Nguyen, H.T., Wing, R.A., Cregan, P., Specht, J., Grimwood, J., Rokhsar, D., Stacey, G., Shoemaker, R.C., and Jackson, S.A. (2010). Genome sequence of the palaeopolyploid soybean. Nature **463,** 178-183.

Sierro, N., Battey, J.N., Ouadi, S., Bakaher, N., Bovet, L., Willig, A., Goepfert, S., Peitsch, M.C., and Ivanov, N.V. (2014). The tobacco genome sequence and its comparison with those of tomato and potato. Nat. Commun. **5,** 3833.

Slotte, T., Hazzouri, K.M., Ågren, J.A., Koenig, D., Maumus, F., Guo, Y.-L., Steige, K., Platts, A.E., Escobar, J.S., Newman, L.K., Wang, W., Mandáková, T., Vello, E., Smith, L.M., Henz, S.R., Steffen, J., Takuno, S., Brandvain, Y., Coop, G., Andolfatto, P., Hu, T.T., Blanchette, M., Clark, R.M., Quesneville, H., Nordborg, M., Gaut, B.S., Lysak, M.A., Jenkins, J., Grimwood, J., Chapman, J., Prochnik, S., Shu, S., Rokhsar, D., Schmutz, J., Weigel, D., and Wright, S.I. (2013). The *Capsella rubella* genome and the genomic consequences of rapid mating system evolution. Nature genetics **45,** 831-835.

The International Wheat Genome Sequencing Consortium, Appels, R., Eversole, K., Stein, N., Feuillet, C., Keller, B., Rogers, J., Pozniak, C.J., Choulet, F., Distelfeld, A., Poland, J., Ronen, G., Sharpe, A.G., Barad, O., Baruch, K., Keeble-Gagnère, G., Mascher, M., Ben-Zvi, G., Josselin, A.-A., Himmelbach, A., Balfourier, F., Gutierrez-Gonzalez, J., Hayden, M., Koh, C., Muehlbauer, G., Pasam, R.K., Paux, E., Rigault, P., Tibbits, J., Tiwari, V., Spannagl, M., Lang, D., Gundlach, H., Haberer, G., Mayer, K.F.X., Ormanbekova, D., Prade, V., Šimková, H., Wicker, T., Swarbreck, D., Rimbert, H., Felder, M., Guilhot, N., Kaithakottil, G., Keilwagen, J., Leroy, P., Lux, T., Twardziok, S., Venturini, L., Juhász, A., Abrouk, M., Fischer, I., Uauy, C., Borrill, P., Ramirez-Gonzalez, R.H., Arnaud, D., Chalabi, S., Chalhoub, B., Cory, A., Datla, R., Davey, M.W., Jacobs, J., Robinson, S.J., Steuernagel, B., van Ex, F., Wulff, B.B.H., Benhamed, M., Bendahmane, A., Concia, L., Latrasse, D., Bartoš, J., Bellec, A., Berges, H., Doležel, J., Frenkel, Z., Gill, B., Korol, A., Letellier, T., Olsen, O.-A., Singh, K., Valárik, M., van der Vossen, E., Vautrin, S., Weining, S., Fahima, T., Glikson, V., Raats, D., Číhalíková, J., Toegelová, H., Vrána, J., Sourdille, P., Darrier, B., Barabaschi, D., Cattivelli, L., Hernandez, P., Galvez, S., Budak, H., Jones, J.D.G., Witek, K., Yu, G., Small, I., Melonek, J., Zhou, R., Belova, T., Kanyuka, K., King, R., Nilsen, K., Walkowiak, S., Cuthbert, R., Knox, R., Wiebe, K., Xiang, D., Rohde, A., Golds, T., Čížková, J., Akpinar, B.A., Biyiklioglu, S., Gao, L., N'Daiye, A., Kubaláková, M., Šafář, J., Alfama, F., Adam-Blondon, A.-F., Flores, R., Guerche, C., Loaec, M., Quesneville, H., Condie, J., Ens, J., Maclachlan, R., Tan, Y., Alberti, A., Aury, J.-M., Barbe, V., Couloux, A., Cruaud, C., Labadie, K., Mangenot, S., Wincker, P., Kaur, G., Luo, M., Sehgal, S., Chhuneja, P., Gupta, O.P., Jindal, S., Kaur, P., Malik, P., Sharma, P., Yadav, B., Singh, N.K., Khurana, J.P., Chaudhary, C., Khurana, P., Kumar, V., Mahato, A., Mathur, S., Sevanthi, A., Sharma, N., Tomar, R.S., Holušová, K., Plíhal, O., Clark, M.D., Heavens, D., Kettleborough, G., Wright, J., Balcárková, B., Hu, Y., Salina, E., Ravin, N., Skryabin, K., Beletsky, A., Kadnikov, V., Mardanov, A., Nesterov, M., Rakitin, A., Sergeeva, E., Handa, H.,

Kanamori, H., Katagiri, S., Kobayashi, F., Nasuda, S., Tanaka, T., Wu, J., Cattonaro, F., Jiumeng, M., Kugler, K., Pfeifer, M., Sandve, S., Xun, X., Zhan, B., Batley, J., Bayer, P.E., Edwards, D., Hayashi, S., Tulpová, Z., Visendi, P., Cui, L., Du, X., Feng, K., Nie, X., Tong, W., and Wang, L. (2018). Shifting the limits in wheat research and breeding using a fully annotated reference genome. Science **361,** eaar7191.

Tuskan, G.A., DiFazio, S., Jansson, S., Bohlmann, J., Grigoriev, I., Hellsten, U., Putnam, N., Ralph, S., Rombauts, S., Salamov, A., Schein, J., Sterck, L., Aerts, A., Bhalerao, R.R., Bhalerao, R.P., Blaudez, D., Boerjan, W., Brun, A., Brunner, A., Busov, V., Campbell, M., Carlson, J., Chalot, M., Chapman, J., Chen, G.-L., Cooper, D., Coutinho, P.M., Couturier, J., Covert, S., Cronk, Q., Cunningham, R., Davis, J., Degroeve, S., Déjardin, A., dePamphilis, C., Detter, J., Dirks, B., Dubchak, I., Duplessis, S., Ehlting, J., Ellis, B., Gendler, K., Goodstein, D., Gribskov, M., Grimwood, J., Groover, A., Gunter, L., Hamberger, B., Heinze, B., Helariutta, Y., Henrissat, B., Holligan, D., Holt, R., Huang, W., Islam-Faridi, N., Jones, S., Jones-Rhoades, M., Jorgensen, R., Joshi, C., Kangasjärvi, J., Karlsson, J., Kelleher, C., Kirkpatrick, R., Kirst, M., Kohler, A., Kalluri, U., Larimer, F., Leebens-Mack, J., Leplé, J.-C., Locascio, P., Lou, Y., Lucas, S., Martin, F., Montanini, B., Napoli, C., Nelson, D.R., Nelson, C., Nieminen, K., Nilsson, O., Pereda, V., Peter, G., Philippe, R., Pilate, G., Poliakov, A., Razumovskaya, J., Richardson, P., Rinaldi, C., Ritland, K., Rouzé, P., Ryaboy, D., Schmutz, J., Schrader, J., Segerman, B., Shin, H., Siddiqui, A., Sterky, F., Terry, A., Tsai, C.-J., Uberbacher, E., Unneberg, P., Vahala, J., Wall, K., Wessler, S., Yang, G., Yin, T., Douglas, C., Marra, M., Sandberg, G., Van de Peer, Y., and Rokhsar, D. (2006). The Genome of Black Cottonwood, Populus trichocarpa (Torr. & Gray). Science **313,** 1596-1604.

Vogel, J.P., Garvin, D.F., Mockler, T.C., Schmutz, J., Rokhsar, D., Bevan, M.W., Barry, K., Lucas, S., Harmon-Smith, M., Lail, K., Tice, H., Schmutz, J., Grimwood, J., McKenzie, N., Bevan, M.W., Huo, N., Gu, Y.Q., Lazo, G.R., Anderson, O.D., Vogel, J.P., You, F.M., Luo, M.-C., Dvorak, J., Wright, J., Febrer, M., Bevan, M.W., Idziak, D., Hasterok, R., Garvin, D.F., Lindquist, E., Wang, M., Fox, S.E., Priest, H.D., Filichkin, S.A., Givan, S.A., Bryant, D.W., Chang, J.H., Mockler, T.C., Wu, H., Wu, W., Hsia, A.-P., Schnable, P.S., Kalyanaraman, A., Barbazuk, B., Michael, T.P., Hazen, S.P., Bragg, J.N., Laudencia-Chingcuanco, D., Vogel, J.P., Garvin, D.F., Weng, Y., McKenzie, N., Bevan, M.W., Haberer, G., Spannagl, M., Mayer, K., Rattei, T., Mitros, T., Rokhsar, D., Lee, S.-J., Rose, J.K.C., Mueller, L.A., York, T.L., Wicker, T., Buchmann, J.P., Tanskanen, J., Schulman, A.H., Gundlach, H., Wright, J., Bevan, M., Costa de Oliveira, A., da C. Maia, L., Belknap, W., Gu, Y.Q., Jiang, N., Lai, J., Zhu, L., Ma, J., Sun, C., Pritham, E., Salse, J., Murat, F., Abrouk, M., Haberer, G., Spannagl, M., Mayer, K., Bruggmann, R., Messing, J., You, F.M., Luo, M.-C., Dvorak, J., Fahlgren, N., Fox, S.E., Sullivan, C.M., Mockler, T.C., Carrington, J.C., Chapman, E.J., May, G.D., Zhai, J., Ganssmann, M., Guna Ranjan Gurazada, S., German, M., Meyers, B.C., Green, P.J., Bragg, J.N., Tyler, L., Wu, J., Gu, Y.Q., Lazo, G.R., Laudencia-Chingcuanco, D., Thomson, J., Vogel, J.P., Hazen, S.P., Chen, S., Scheller, H.V., Harholt, J., Ulvskov, P., Fox, S.E., Filichkin, S.A., Fahlgren, N., Kimbrel, J.A., Chang, J.H., Sullivan, C.M., Chapman, E.J., Carrington, J.C., Mockler, T.C., Bartley, L.E., Cao, P., Jung, K.-H., Sharma, M.K., Vega-Sanchez, M., Ronald, P., Dardick, C.D., De Bodt, S., Verelst, W., Inzé, D., Heese, M., Schnittger, A., Yang, X., Kalluri, U.C., Tuskan, G.A., Hua, Z., Vierstra, R.D., Garvin, D.F., Cui, Y., Ouyang, S., Sun, Q., Liu, Z., Yilmaz, A., Grotewold, E., Sibout, R., Hematy, K., Mouille, G., Höfte, H., Michael, T., Pelloux, J., O'Connor, D., Schnable, J., Rowe, S., Harmon, F., Cass, C.L., Sedbrook, J.C., Byrne, M.E., Walsh, S., Higgins, J., Bevan, M., Li, P., Brutnell, T., Unver, T., Budak, H., Belcram, H., Charles, M., Chalhoub, B., Baxter, I., The International Brachypodium, I., Principal, i., sequencing, D.N.A., assembly, Pseudomolecule, a., sequencing, B.A.C.e., Transcriptome, s., analysis, Gene, a., annotation,

Repeats, a., Comparative, g., Small, R.N.A.a., Manual, a., and gene family, a. (2010). Genome sequencing and analysis of the model grass *Brachypodium distachyon*. Nature **463,** 763-768.

Wan, T., Liu, Z.-M., Li, L.-F., Leitch, A.R., Leitch, I.J., Lohaus, R., Liu, Z.-J., Xin, H.-P., Gong, Y.-B., Liu, Y., Wang, W.-C., Chen, L.-Y., Yang, Y., Kelly, L.J., Yang, J., Huang, J.-L., Li, Z., Liu, P., Zhang, L., Liu, H.-M., Wang, H., Deng, S.-H., Liu, M., Li, J., Ma, L., Liu, Y., Lei, Y., Xu, W., Wu, L.-Q., Liu, F., Ma, Q., Yu, X.-R., Jiang, Z., Zhang, G.-Q., Li, S.-H., Li, R.-Q., Zhang, S.-Z., Wang, Q.-F., Van de Peer, Y., Zhang, J.-B., and Wang, X.-M. (2018). A genome for gnetophytes and early evolution of seed plants. Nat. Plants **4,** 82-89.

Wang, S., Li, L., Li, H., Sahu, S.K., Wang, H., Xu, Y., Xian, W., Song, B., Liang, H., Cheng, S., Chang, Y., Song, Y., Çebi, Z., Wittek, S., Reder, T., Peterson, M., Yang, H., Wang, J., Melkonian, B., Van de Peer, Y., Xu, X., Wong, G.K.-S., Melkonian, M., Liu, H., and Liu, X. (2020). Genomes of early-diverging streptophyte algae shed light on plant terrestrialization. Nat. Plants **6,** 95-106.

Wickell, D., Kuo, L.-Y., Yang, H.-P., Dhabalia Ashok, A., Irisarri, I., Dadras, A., de Vries, S., de Vries, J., Huang, Y.-M., Li, Z., Barker, M.S., Hartwick, N.T., Michael, T.P., and Li, F.-W. (2021). Underwater CAM photosynthesis elucidated by Isoetes genome. Nat. Commun. **12,** 6348.

Worden, A.Z., Lee, J.-H., Mock, T., Rouzé, P., Simmons, M.P., Aerts, A.L., Allen, A.E., Cuvelier, M.L., Derelle, E., Everett, M.V., Foulon, E., Grimwood, J., Gundlach, H., Henrissat, B., Napoli, C., McDonald, S.M., Parker, M.S., Rombauts, S., Salamov, A., Von Dassow, P., Badger, J.H., Coutinho, P.M., Demir, E., Dubchak, I., Gentemann, C., Eikrem, W., Gready, J.E., John, U., Lanier, W., Lindquist, E.A., Lucas, S., Mayer, K.F.X., Moreau, H., Not, F., Otillar, R., Panaud, O., Pangilinan, J., Paulsen, I., Piegu, B., Poliakov, A., Robbens, S., Schmutz, J., Toulza, E., Wyss, T., Zelensky, A., Zhou, K., Armbrust, E.V., Bhattacharya, D., Goodenough, U.W., Van de Peer, Y., and Grigoriev, I.V. (2009). Green evolution and dynamic adaptations revealed by genomes of the marine picoeukaryotes *Micromonas*. Science **324,** 268-272.